THE EFFECT OF FRESHWATER INPUT ON $\delta^{18}O$ DISTRIBUTION AT THE YOUNGER DRYAS

by

ANAND SONI

Presented to the Faculty of the Graduate School of

The University of Texas at Arlington in Partial Fulfillment

of the Requirements

for the Degree of

MASTER OF SCIENCE, GEOLOGY

THE UNIVERSITY OF TEXAS AT ARLINGTON

May 2014

Acknowledgements

Firstly, I would like to thank Arne Winguth for his continuous guidance and support and for motivating me to complete my Master's thesis. I would particularly like to thank him for the patience with which he answered my questions and keeping me focused throughout.

I would particularly like to thank Taylor Hughlett for teaching me the programming knowhow required and most importantly for sharing the results from her CCSM3 Younger Dryas simulations. Apart from the constant interactions with Dr. Winguth, discussions with Angela Osen and Taylor Hughlett have been insightful and helped with many comments to improve the thesis.

I appreciate the feedback offered by the entire climate research group supervised by Dr. Arne Winguth, especially Dr. Cornelia Winguth, who always provided constructive and meticulous comments to enhance the thesis. Advice and comments from Dr. Qinhong Hu have also been a great help.

This research has been supported by NSF grant EAR 09-03071.

December 18, 2013

Abstract

THE EFFECT OF FRESHWATER INPUT ON $\delta^{18}O$ DISTRIBUTION

AT THE YOUNGER DRYAS

Anand Soni, Master's Thesis

The University of Texas at Arlington, 2014

Supervising Professor: Arne Winguth

The Younger Dryas cooling event (~12.9–11.5 $\delta^{18}O$ ka BP) is a recognized example of an abrupt decline of the Atlantic meridional overturning circulation and thus may serve as an analog for expected rapid future climate change. Prediction of the atmospheric and oceanic conditions at the onset of Younger Dryas presents various challenges and this study is aimed to contribute towards the better understanding of the changes in the oceanic tracer distribution.

Here, output from a fully coupled coarse resolution model from the National Center of Atmospheric Research, the Community Climate System Model version 3 (CCSM3) have been utilized to predict diagnostically the oxygen isotope ratio relative to standard mean ocean water $\delta_{w.}$ By using an inverse paleotemperature equation, distribution of oxygen isotopes in carbonate shells δ_c can be predicted. While present-day CCSM3 simulation of δ_w generally agree with observations from the World Ocean Circulation Experiment, a significant bias occurs for the North Atlantic benthic isotope data δ_c plot with a mean error of 1.73 ‰. For the Younger Dryas the distribution of two scenarios have been analyzed. The first with present-day freshwater input and the second with Northern Hemisphere fresh forcing. Comparison of simulated δ_c with observed benthic stable oxygen isotope data suggest that changes in freshwater forcing need to be considered in order to explain the oxygen isotopic distribution of the Younger

Dryas. The approximated prediction of δ_w and lack of data for the North Atlantic subsurface suggest significant uncertainties.

Table of Contents

List of Illustrations

List of Tables

Chapter 1

Introduction

The Younger Dryas stadial was a geologically period (~12.9 – 11.5 δ^{18}O ka BP) after the last glacial maximum (21 ka BP) that is characterized by an abrupt shift in the climate, leading to a cold period, predominantly affecting the Northern Hemisphere, and that has characteristic similarity to Dasngaard-Oeschger (DO) oscillations seen in the Greenland ice core record (Stuiver and Grootes, 2000; Mangerud et al., 2009) (Figure 1-1).

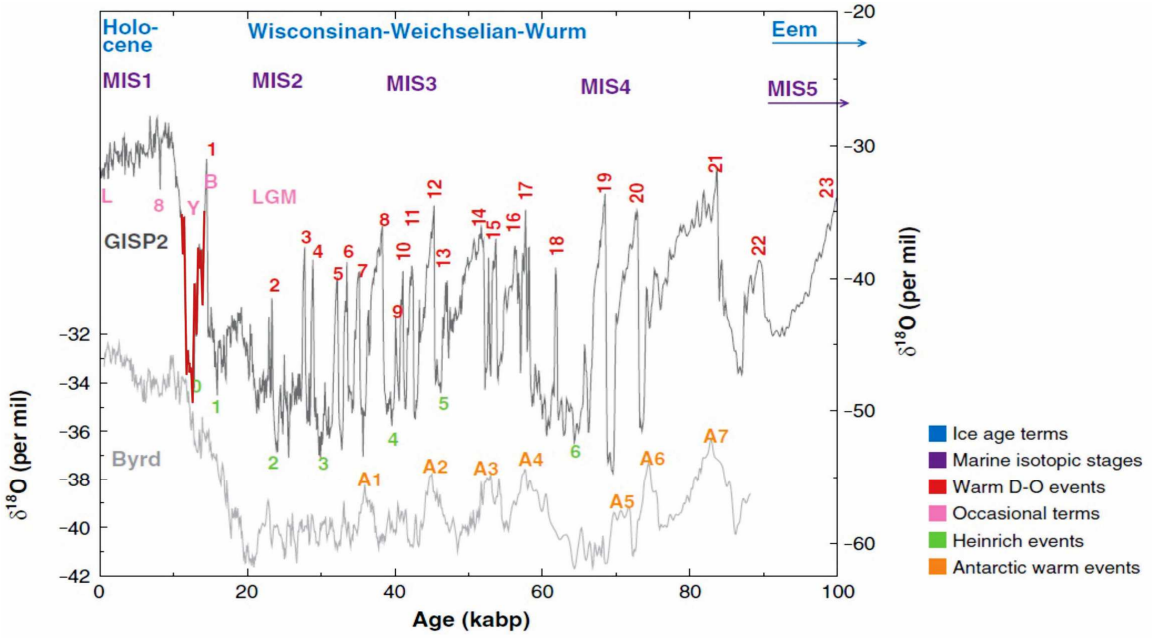

Figure 1-1 δ^{18}O record from GISP2 (Greenland Ice Sheet Project 2) and Byrd Station, Antarctica. Y = Younger Dryas, also highlighted in red. (from Alley, 2007).

Evidences for the Younger Dryas are present in the form of from δ^{18}O record from GISP2 (Greenland Ice Sheet Project 2; Fig 1-1), polar foraminifera indicating a southward readvance of polar water to the North Atlantic (Ruddiman et.al., 1977), Scotland tree pollen records pointing to reversal towards Arctic vegetation in Europe

(Coope and Lemdahl, 1995), fossil insect population indicating a return to cooler temperature (Atkinson, 1987), stable carbon isotope data (Sarnthein et al., 1994), and modeling studies (Peltier et al., 2006; Liu et al., 2009). The ice sheets during this cold event covered much of the Northern Hemisphere above 40° N latitude, which included Greenland, most of Europe and the Laurentide Ice Sheet covering approximately one-third of the North American continent. The Younger Dryas followed the warm Bølling-Allerød interstadial during the last deglaciation and is among the most extensively studied events of the recent geological past (Peltier et al., 2006). A complete understanding of the sequence of events leading to the Younger Dryas oscillation is still controversial. A number of compelling theories, discussed later in the chapter, have been put forward to explain the sequential triggering mechanism that could have led to sudden climatic shift at the Younger Dryas. One of the more commonly accepted hypotheses considers abrupt changes in the Atlantic thermohaline circulation.

One of the key factors responsible for the change in the state of the Atlantic thermohaline circulation is the increase in amount of greenhouse gases in the atmosphere, in particular, carbon dioxide (CO_2). Figure 1-2 shows the secular trend in the atmospheric CO_2 as recorded at the Mauna Loa Observatory since 1958 which represents the man-made emissions along with the seasonal cycles and the inter-annual variations. The reason for the crests and troughs in the CO_2 record is the uneven distribution of land masses on either side of the equator. The Northern hemisphere, consisting majority of the land mass and vegetation, when titled towards the sun (summer/spring), absorbs CO_2 and when tilted away (winter/fall), releases CO_2. Hence, each pair of crest and trough represents a one year cycle.

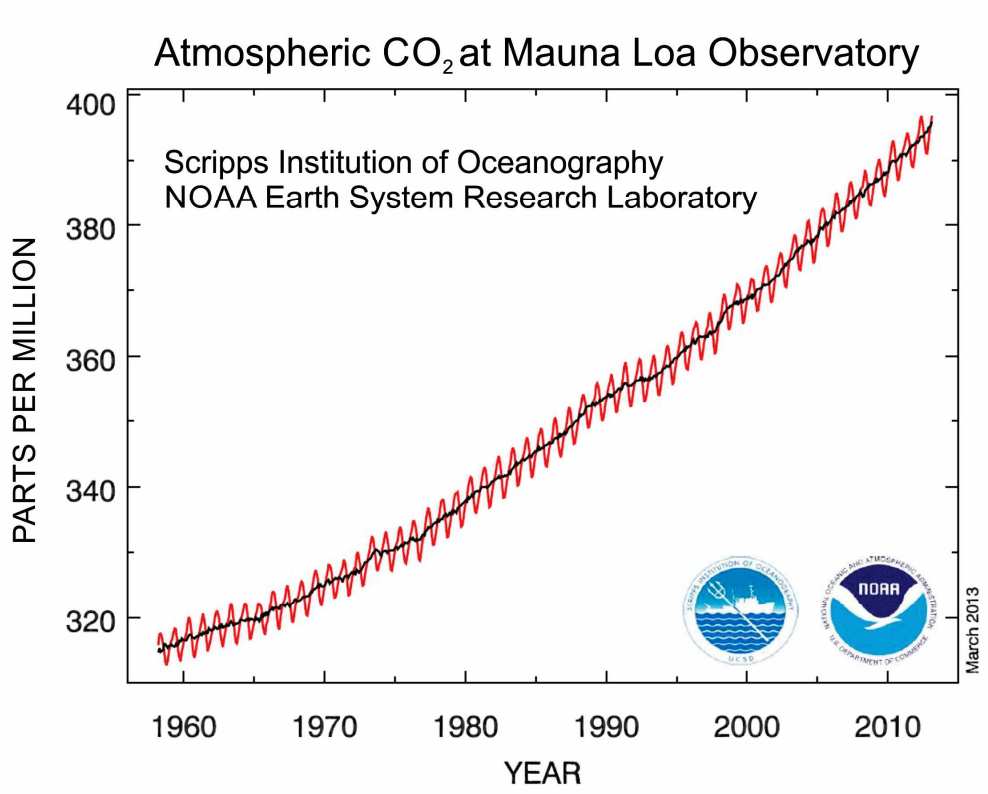

Figure 1-2 Atmospheric CO_2 at the Mauna Loa observatory, Hawaii (Current CO_2 concentration – 396.80 ppm as of February 2013, Latitude: 19.539, Longitude: 155.578, Elevation: 3397 m, Time Zone: GMT-10) (from www.esrl.noaa.gov/gmd).

The amount of atmospheric CO_2 as of February 2013 is 396.80 ppm which is considerably higher than the natural range over the past 650,000 years (180 to 300 ppm) (IPCC 2007). An increase in the amount of CO_2, and hence CO_2 radiative forcing would enhance climate change and variability. For example, an increase in transport of water vapor through higher evaporation rates at the lower latitudes with a global warming increases the in amount of net precipitation at higher latitudes and hence reduces strength of the North Atlantic overturning circulation (IPCC, 2007) due to freshening of the Atlantic, leading to an analog scenario comparable to the Younger (Figure 1-2).

Although the varying scenarios show a different pattern, there is an overall decline in the strength of the thermohaline circulation with the predicted rate of increase of the greenhouse gases.

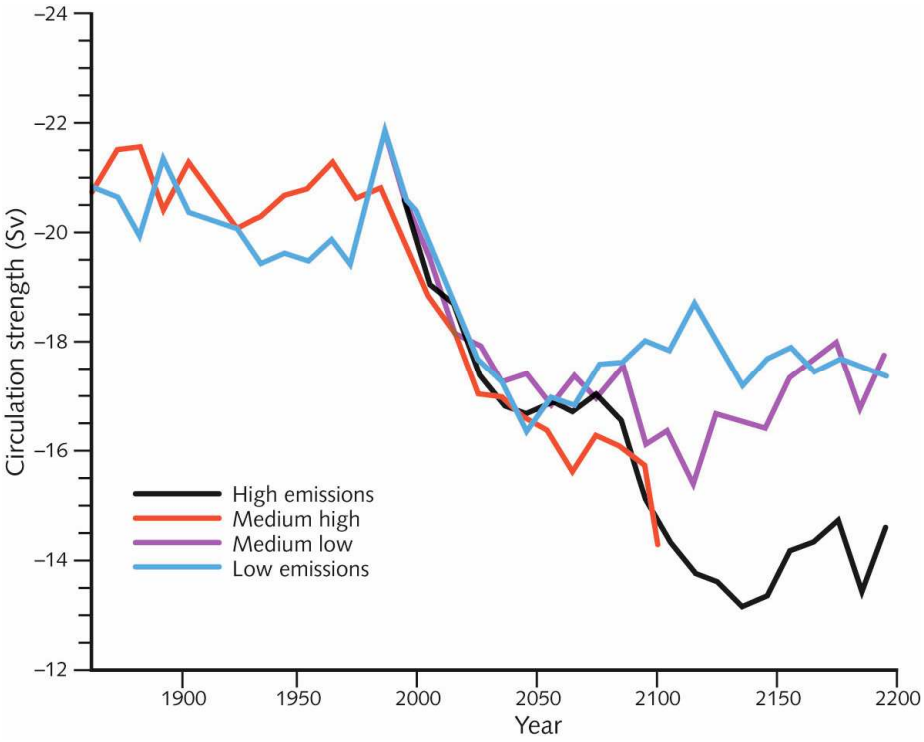

Figure 1-3 Change in the strength of the thermohaline circulation (THC) in the North Atlantic as simulated by the Hadley Centre climate model for four SRES (Special Reports on Emission Scenarios).

One of the leading hypotheses that have been put forward to explain this sudden shift to a cold period is the abrupt coupled changes of the North Atlantic Deep Water (NADW) formation, North Atlantic sea ice extent and concerned climatic conditions in response to the varying fresh water fluxes (Rooth 1982). Analysis of paleoclimate data from various sources (Broecker et al., 1985) suggest that extensive freshwater input to the North Atlantic would reduce the rate of the Atlantic Meridional Overturning Circulation

(AMOC) sinking, trigger sea ice growth in the GIN seas (Greenland, Icelandic and Norwegian seas) and ultimately result in global scale climate anomalies (Alley, 2007).

The following three different pathways have been suggested as outlets for the Lake Agassiz floodwater: (1) The southern Mississippi route (Broecker et al. (2006) (2) The eastern St. Lawrence route (Rooth, 1982 and Broecker et al. 2006) (3) The northeastern Hudson Strait route (Andrews and MacLean 2003). Broecker et al. (2006) suggested that a catastrophic release of fresh water from Lake Agassiz could have served as a probable reason for the onset of the Younger Dryas, but lack of any geomorphic evidences suggesting rather an alternate route for the flood water through Lake Superior via St. Lawrence lowlands into the Northern Atlantic. Recently, Murton et al. (2010) inferred from evidence in the form of a regional erosion surface, gravels and OSL dates that the freshwater input from the Mackenzie River into the Arctic Ocean occurred around 13,000 years ago, near the onset of the Younger Dryas. This Arctic route would also justify the absence of geomorphic changes of the southern Mississippi and the eastern St Lawrence River (Broecker et al., 2006). Moreover, the most significant discharge into the Arctic Ocean (mean values of 1.0-2.2 dSv) is recorded at the onset of the Younger Dryas and is believed to have been predominantly responsible for the shutdown of the thermohaline circulation (Tarasov and Peltier, 2005). It is also noticeable that, on the basis of stable isotopes and CO_2 records in Antarctic ice cores, that the Younger Dryas, instead of being a random one-time event that accompanied the termination of the cold period, was rather an extremely important event of the last deglaciation (Broecker et al., 2010). Bakke et al. (2009) came to a similar conclusion inferred from multiple proxies from two sediment records from Lake Krakenes and Nordic seas, their study concluded that rapid alternations between (i) influx of warm-salty North Atlantic water (causing northward drifting of the westerly wind system and consequent

melting of glaciers) and (ii) sea-ice cover because of input of the freshwater from the glaciers melting, thus deflecting westerly wind belts more southward and causing subsequent cooling, that could have resulted in the termination of Younger Dryas. Eisenman et al. (2009), based on global climate model studies, proposed an alternative to the fresh water flood hypothesis, stating that increased precipitation owing to receding glacial ice led to a diminished overturning circulation and resulted in positive feedback loop which increased the sea ice extent and consequently lowered the temperature significantly.

One of the controversial theories suggests that a cluster of comets or carbonaceous chondrites created numerous air-shocks and possible terrestrial impacts in North America around 12,900 years ago on the basis of the presence of nanodiamonds (Kennett et al., 2008). Other lines of evidences include unusually high amount of magnetic microspherules, iridium and proxies for wildfires (Firestone et al., 2007). However, Tian et al. (2011) concluded that the presence of nanodiamonds is not a conclusive evidence to support the impact theory and that related evidences could possibly be formed by alternate processes. An independent investigation conducted by Surovell et al. (2009) wherein they investigated seven different sites, including two by Firestone et al., (2007) did not return similar results. Recently, a review of the impact hypothesis (Pinter et al., 2011) supports a catastrophic extraterrestrial event. Seven out of twelve signatures of an impact have been verified to be non-reproducible and the remaining ones point towards either a non-catastrophic mechanism or a terrestrial source. LeCompte et al. (2012) conducted an independent blind investigation of the same survey by Surovell et al. (2009) and Firestone et al. (2007) and concluded that the reason for the inconsistency in the results was owing to a difference in investigative procedure and rendered it inconclusive. In the following chapter we will focus on the less

controversial YD hypotheses which are related to changes in the meltwater pulses into the North Atlantic Ocean.

Chapter 2

Oxygen Isotopes

The objective of the study is to predict oxygen isotope ratios diagnostically from simulated temperature and salinity compiled by Community Climate System Model version 3.0 (CCSM3) to validate the rapid climate fluctuations during the Younger Dryas and compare the predicted $\delta^{18}O$ values with the observations. Liu et.al (2009), using NCAR CCSM3 model, carried out the first synchronously coupled simulation from Last Glacial Maximum (LGM) to the Bølling-Allerød (BA) warming. The results of the simulations were found to be in accordance with the observations (amplitude of simulated BA being comparable to amplitude reconstructed from paleoclimate proxies), reproducing key features of deglacial climate evolution.

Small differences in the thermodynamic properties of isotopes lead to a temperature dependency in the fractionation of isotopes (Urey, 1947). This concept can be utilized for paleoclimate study. There are three naturally occurring isotopes of oxygen, ^{16}O, ^{17}O and ^{18}O. ^{18}O is the heaviest (17.999160 amu) and the second most rare (0.200% by number) of the three isotopes of oxygen. The presence of a heavier isotope (^{18}O) of an element in a molecule decreases the vibration and energy and increases the strength of the covalent bonds along with stability when it replaces a lighter isotope (^{16}O, ^{17}O). Molecules containing heavier isotopes are more stable and consequently less reactive, particular for isotopes in gases, but not for isotopes in liquids or ionic crystals. At constant temperature, velocity of the water molecules containing ^{16}O is greater than the velocity of the water molecules containing ^{18}O. This effect of mass of the isotope on velocity and stability of the water molecule is the basis of the fractionation of oxygen isotopes during the evaporation-condensation process. The relative rarity of ^{18}O to the common isotope ^{16}O in ordinary sea water and the temperature dependency of the ^{18}O:^{16}O ratio in sea

water, owing to the preferential evaporation of ^{16}O at the expense of ^{18}O, make it a suitable tracer for the oceanic flow patterns and other related quantitative analysis. An understanding of the following terms helps us to quantify the variations in the oxygen isotope ratios in a better way.

2.1 Isotope Ratio

The relative portions of oxygen$^{18}O/^{16}O$ isotope ratio, expressed as 'R', is the isotopic composition of all elements whose isotopes are fractionated and can be defined according to (Craig, 1961) as follows:

$$R = \frac{^{18}\text{O (isotopic abundance of heavy isotope)}}{^{16}\text{O(isotopic abundance of light isotope)}} = \frac{0.200}{99.762} = 0.002004$$

2.2 Isotope Fractionation Factor

The isotope fractionation factor 'α' is defined in order to quantify this fractionation. The isotope fractionation that takes place during the change in state from either solid to liquid or from liquid to gas is expressed according to Gunter Faure (2004) as:

$$\alpha_g^l = \frac{R_l}{R_v}$$

Here, α_g^l is the Isotope fractionation factor (for phase change from liquid to gas), R_l is the isotope ratio of H_2O in liquid phase and R_v is the isotope ratio of H_2O in gas phase. As the ratio is mostly expressed in terms of 'solid to liquid' or 'liquid to gas', it is mostly greater than one depending on the temperature. The fractionation factor approaches 1 as it decreases with the increase in temperature and ceases as it approaches high values.

2.3 $\delta^{18}O$ (Delta-18-O)

The ratio of oxygen isotope ration of standard mean ocean water (SMOW), $\delta^{18}O_{SMOW}$, is expressed as

$$\delta^{18}O_{SMOW} = \frac{R_{sample} - R_{SMOW}}{R_{SMOW}} 10^3 \ [‰]$$

The resulting values are expressed in per mil (‰, one part per thousand) units. Negative values indicate that the sample has lower ratio of ^{18}O:^{16}O (depleted in ^{18}O relative to standard) and positive values indicate that the sample has higher ratio of ^{18}O:^{16}O (enriched in ^{18}O relative to standard). Hence, in any given sample of water, the oxygen of the sample is always determined in terms of the amount of heavy isotope relative to the standard (SMOW). In order to avoid confusion, isotopic composition of oxygen in a sample is always expressed in terms of enrichment or depletion of ^{18}O (heavy isotope) and not $\delta^{18}O$. As sited in the coming discussion, a similar standard (PDB-1) for the isotopic studies based on carbonate fossils has been formulated from a Cretaceous belemnite found in the PeeDee Formation of North Carolina. There is a difference of +0.2 ‰ in the CO_2 released from PDB-1 as compared to CO_2 calculated with SMOW (Craig, 1961).

The standard R_{SMOW} is based on a set of ocean water samples from the Atlantic, Pacific and Indian Ocean (sample depth: 500 to 2000 m, no-direct dilution by continental runoff or glacial melt water) used by Epstein and Mayeda (1953) to obtain a universally accepted standard for ^{18}O data so that isotopic analysis in different laboratories could be comparable. The sample used to derive this relation is a distilled water sample provided by the United States National Institute of Standards and Technology (NIST-1) and not a definite ocean water sample.

2.4 Oxygen Isotope Cycle

There is a continual exchange of oxygen isotopes between the ocean-atmosphere systems through evaporation and condensation, due to the poleward moisture transport from the equator to the poles.

$\delta^{18}O$ records, mainly from the ice cores of Arctic and Antarctic, have proved to be valuable for temperature reconstruction. Temperature has a direct correlation with the variations in the ratio of the oxygen isotopes (Urey, 1947). Figure 2-1 shows the process of isotopic differentiation of water vapor during its transport from the tropics to the Antarctic ice-sheets. The $\delta^{18}O$ values are closer to the mean oceanic value near the tropics, but closer to the higher latitudes there is a decrease in evaporation due to the decline in temperature. As the vapor moves poleward, there is a net depletion of the heavier isotopes because during the condensation, heavier isotopes are enriched in the rain droplets. Thus, the remaining vapor becomes lighter and leads to a decrease of $\delta^{18}O$ with latitude. The mean $\delta^{18}O$ value of around ~-40 ‰ on the over Antarctica coast and this is further reduced due to negligible evaporation from the surface of the ice sheets.

The heavier $H_2{}^{18}O$ is removed first during precipitation, and the water vapor gets $H_2{}^{16}O$ enriched. This fractionation process, also known as Rayleigh's fractionation, depends on the temperature, i.e. with the decline in temperature the precipitation gets depleted in $\delta^{18}O$. The greater the fall in temperature, higher the amount of condensation and lower will be the ^{18}O concentration relative to the original water source. Thus, temperature of condensation primarily controls the isotopic concentration in water droplet or ice particle. $\delta^{18}O$ records have also been used for salinity reconstruction. Increase in evaporation leads to the increase in salinity of the surface water and to increase in $\delta^{18}O$. Thus, $\delta^{18}O$ and salinity are in first order linear correlated (Figure 2-2).

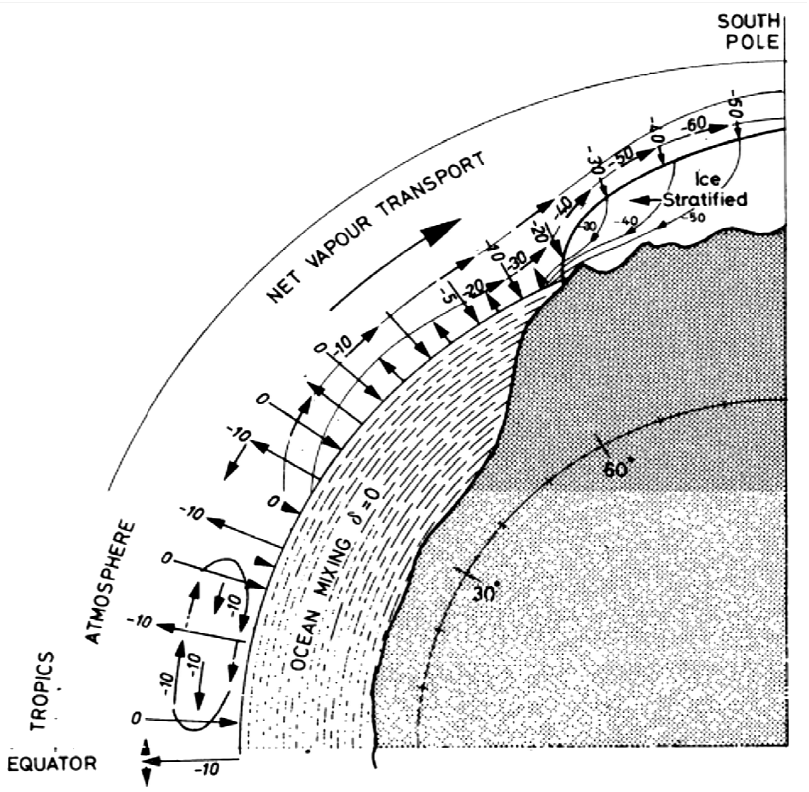

Figure 2-1 Schematic presentation of isotopic cycle of water vapor from the tropical ocean to the Antarctic ice sheet. A -10 value for $\delta^{18}O$ indicates that the sample has an ^{18}O:^{16}O ratio of 1 % (or 10 ‰) less than SMOW. (Figure from Robin, 1977)

2.5 $\delta^{18}O_{SMOW}$ Inferred from Salinity

The first part of this study includes producing a set of data from $\delta^{18}O$ of Benthic Foraminifera δ_c from ODP cores (Ocean Drilling Program) and comparing it with available simulated $\delta^{18}O_{SMOW}$ values using equation (2-2). δ_w can be inferred from a linear regression to salinity as derived from surface (0-250 m) and subsurface water masses (250-1000 m) of the GEOSECS stations in the North Atlantic (Figure 2-2; Östlund et al. 1987; Labeyrie et al., 1992).

(2-1)

There is a change in the behavior of temperature, salinity of water and foraminiferal $\delta^{18}O$ with a change in the location where the water is formed.

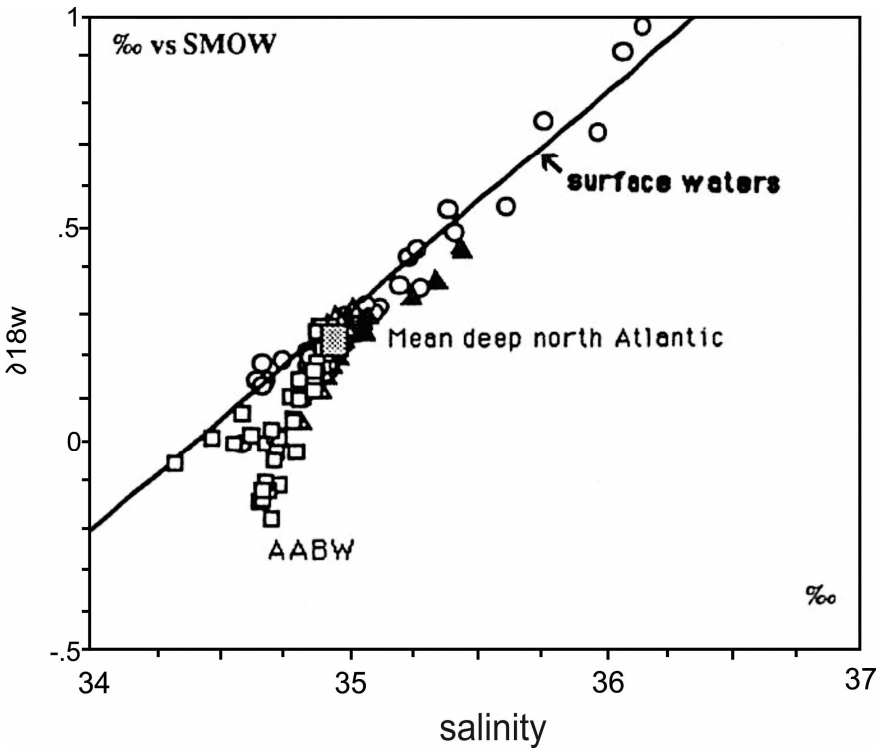

Figure 2-2 Distribution of water $\delta^{18}O$ and salinity for GEOSECS Atlantic stations (Labeyrie et al., 1992).

2.6 Oxygen Isotopes in Seawater and Calcium Carbonate ($CaCO_3$)

The uptake of oxygen isotopes in calcareous marine fauna depends on temperature in which the slow crystallization of $CaCO_3$ by marine microfauna (e.g. benthic foraminifera) in water leads to the $\delta^{18}O$ being slightly higher in the calcium carbonate as compared to the water. With the increase in the water temperature the difference of the oxygen isotopes between the $CaCO_3$ of the shells and the water reduces (Urey, 1948). These disequilibrium effects are well established for benthic foraminifera (Duplessy et al., 1970, Belanger et al., 1981, McCorkle et al., 1985, etc.) and

are approximately constant through space and time. However, marginally variable disequilibrium effects in benthic foraminifera may not be discarded.

On the basis of experiments and observed data which correlate the isotopic composition of calcium carbonate deposited by the marine organisms to the temperature (T) at the time of deposition, the following relation has been approximated. There are variations to this relation based on the type of technique used and on the fractionation temperature (Shackleton, 1974; Mix, 1987).

$$T = 16.9 - 4.2(\delta_c - \delta_w) + 0.13(\delta_c - \delta_w)^2 \quad (2\text{-}2)$$

The water temperature (T) is in degree Celsius, δ_c is the difference between sample carbonate and SMOW standard, and $\delta^{18}O_{SMOW}$ (δ_w) is the difference between the $\delta^{18}O$ of water, in which the sample was precipitated and SMOW (Epstein and Mayeda, 1953; Craig, 1965). (δ_w) to be determined by the following equation (Shackleton 1974; Mix 1987).

The glacial and deglacial of $\delta^{18}O$ values in ocean water (i.e. increase in the ratio of ^{18}O:^{16}O in ocean during glacial periods and a decrease during deglaciation) resulting in complications in temperature.

The role of metabolically produced carbonate tests by living organisms leads to isotopic disequilibrium with the water, resulting in a departure of $\delta^{18}O$ from the thermodynamically predicted values. Narrowing down the selection of species and modifying the measured isotopic values accordingly can prove to be a solution to this problem. In case of the planktic foraminifera, an uncertainty arising from the variations in depth habitat is another complication involved in calculating water temperature from the isotopic composition of carbonate tests.

Changes in the $\delta^{18}O$ values may also be linked to a large scale dilution from melting of ice-sheets and to local changes in the precipitation-evaporation relationship. Contrary to the equatorial waters where the amount of ^{18}O and ^{16}O isotopes remains balanced due to the return of evaporated water as run-off or precipitation, the ^{16}O that gets evaporated near the poles precipitates and is stored in the ice sheets. Hence, the ice sheets become rich in ^{16}O, whereas the ocean water near the poles gets enriched in ^{18}O due to the lack of ^{16}O returning back to balance it. Apart from run-off and precipitation, two important delayed responses through ice calving from continental ice sheets and release of fossil water from aquifers also affect the ^{18}O:^{16}O ratio. A fossil isotopic signature with lower $\delta^{18}O$ values is introduced in the ocean through these two processes which is inconsistent with the present day freshwater cycle and introduces an error in the quantitative evaluation of isotopes. All the above mentioned factors including many more have to be kept in mind when dealing with isotopic calculations.

2.7 Predicted δ_c from Simulated Temperature and Salinity

Using the temperature, salinity and δ_w relationships mentioned earlier, we come up with a formula for the predicted δ_c. One can predict δ_c from simulated temperature and salinity from CCSM-3. δ_w can be inferred from a linear regression to salinity as derived from surface (0-250 m) and subsurface water masses (250-1000 m) of the GEOSECS stations in the North Atlantic (Figure 2.2; Östlund et al., 1987; Labeyrie et al., 1992)

The values of constants S_o and δ_o can be taken as 34.9 and 0.26 respectively (Labeyrie et al., 1992). Equation (2-2) can be rearranged for δ_c and replacing δ_w as function of temperature as per equation (2-1), we get the following solution:

$$\delta_c = \left[\frac{4.2 \pm \sqrt{(8.852 - 0.52T)}}{0.26}\right] + \delta_w \qquad (2\text{-}3)$$

Chapter 3

Objectives

In this study, oxygen isotopes will be predicted from temperature and salinity profiles to investigate the climatic changes during the Younger Dryas. Stable oxygen isotopes have also been used as tracers for delineating hydrological flow-paths on the basis of variations in freshwater pulses from continental ice sheets. This will assess different sources of fresh water that could have led to the shutdown of the Atlantic Meridional Overturning Circulation (AMOC) during the Younger Dryas. The aim of this study is to help in better understanding the distribution of $\delta^{18}O$ as a tracer in the ocean and the factors affecting this distribution.

As mentioned previously, Murton et al., 2010 presented evidence in the form of regional erosion surface, gravels and OSL dates (13,000 ka) of a Mackenzie River flood (into the Arctic Ocean, Figure 3-1) to support the Broecker et al., 2006 hypothesis of destructive fresh water flood from Lake Agassiz leading to the onset of Younger Dryas. In contrast, Tarasov and Peltier (2005) hypothesize that a massive Arctic fresh water flux (mean values of 1.0-2.2 dSv) into the GIN (Greenland-Iceland-Norwegian) seas via the Fram Strait as a triggering factor for the Younger Dryas. An alternative hypothesis proposed by Eisenman et al. (2009) suggest that increased precipitation induced a positive feedback mechanism resulting in increased sea ice extent and the consequent decline in temperature. There is a lack of a unifying theory to explain the freshening of the North Atlantic. A quantitative study of the effect of freshwater forcing mechanisms is required.

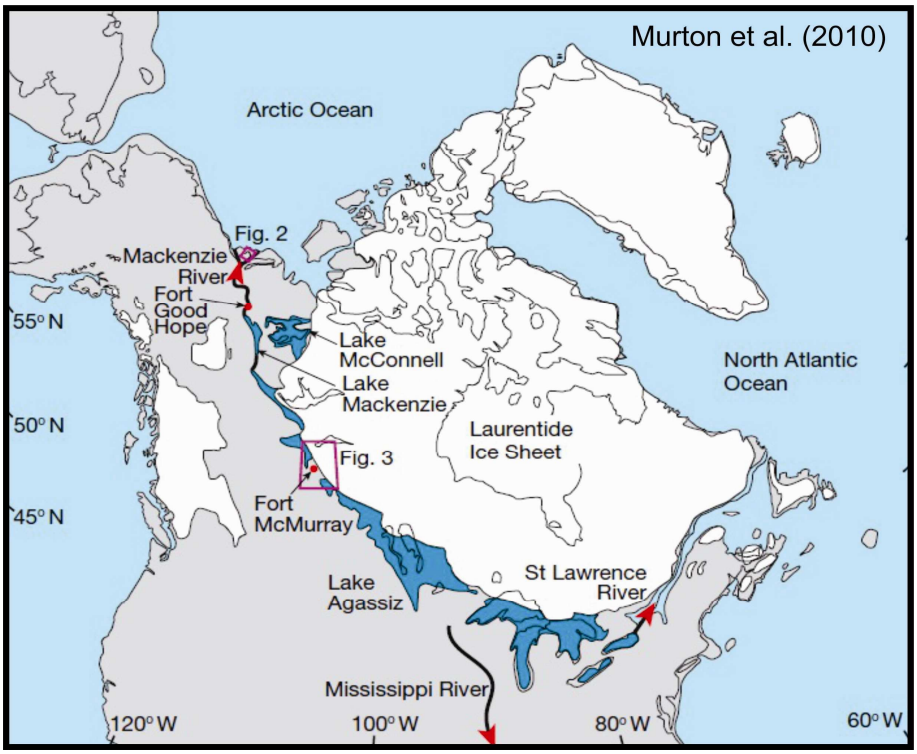

Figure 3-1 Ice cover and large proglacial ice lakes near the start of Younger Dryas along with the three probable outlets are depicted (Murton et al, 2010)

Hence, the current study is aimed to pursue the following objectives:

1. To determine the influence of changes in runoff of melt-water on the shutdown of the AMOC that led to the onset of the Younger Dryas.

2. To investigate the strength of the freshwater pulses from the different sources (Mississippi River, Labrador Sea, McKenzie River) by comparing oxygen isotopes from sedimentary deep sea records and oxygen isotopes simulated with a comprehensive climate model.

Chapter 4

Model Description

4.1 The Community Climate System Model (CCSM3)

The model used in this study is the Community Climate System Model version 3.0 (CCSM3) which is a coupled climate model (Figure 4-1) consisting of (i) the Community Atmosphere Model version 3 (CAM3), which is a three-dimensional general model of the atmosphere solved with the spectral method in the horizontal and consisting of 26 vertical levels (Collin et al., 2006a.), (ii) the Community Land Model (CLM3), which employs the same grid as the atmospheric general circulation model along with a river routing scheme including land cover and plant functional types in each grid cell (Dickinson et al. 2006), (iii) the Parallel Ocean Program (POP), a three dimensional model of general circulation of the ocean in vertical z-coordinates and (iv) the Community Sea Ice Model (CSIM), a dynamic-thermodynamic ice model consisting a subgrid-scale ice thickness distribution and the energy conserving thermodynamics of Bitz and Lipscomb (1999), with each thickness category consisting of four ice layers and one snow layer along with the elastic-viscous-plastic rheology of Hunke and Dukowicz (1997). These four components exchange fluxes through a central coupler component (CPL6). This arrangement allows every component to be created, altered or substituted individually.

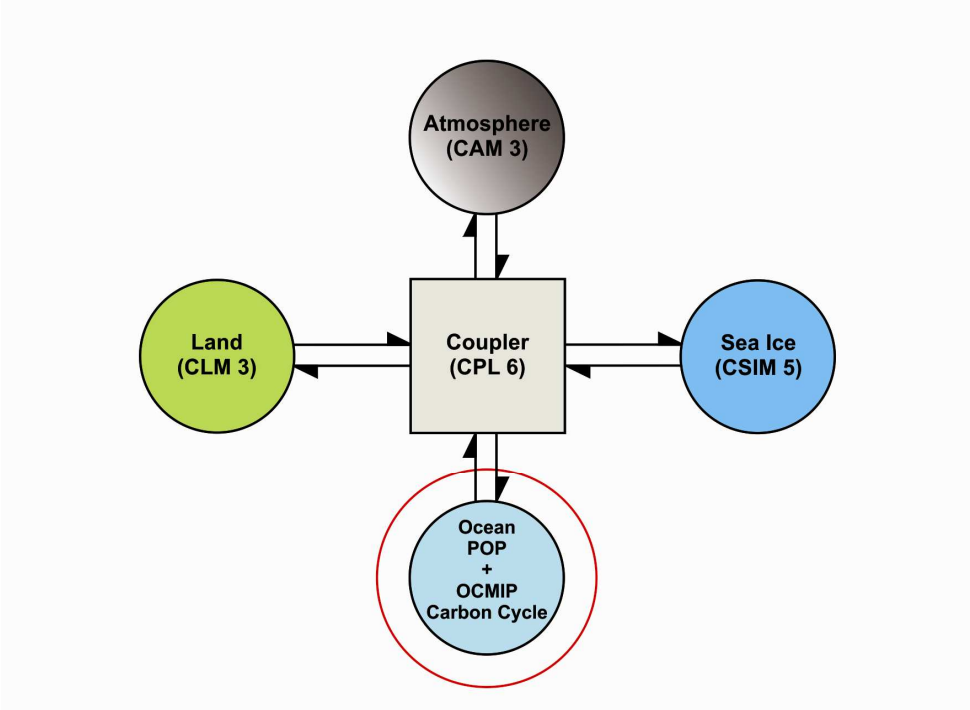

Figure 4-1 Schematic presentation of the land (CLM 3), atmosphere (CAM 3), sea ice (CSIM 5) and the ocean (POP) components interacting with the coupler in CCSM3

Several improvements have been made to eliminate biases produced by previous editions of the model (Collins et al., 2006); however, uncertainties remain such as in the prediction periodicity and total variance of ENSO (El Niño Southern Oscillation), and tropical precipitation pattern. The horizontal resolution for the atmosphere is T31 (latitude longitude grid: 3.75°x3.75°) and for the ocean is 3° (nominal resolution) (Yeager et al., 2006). The atmospheric model has 26 vertical levels and the ocean model has 25 vertical z-coordinate levels.

4.2 The Ocean Carbon Cycle Model

An adapted version of the Ocean Carbon Cycle Model Inter-comparison Project (OCMIP) (Doney et al., 2006; Najjar and Orr, 1999, http://www.ipsl.jissieu.fr/OCMIP/) is used in conjunction with CCSM3 to simulate the carbon cycle for the Younger Dryas. The

model predicts air-sea fluxes of CO_2 with the wind-dependent gas exchange coefficient (Wanninkhof, 1992) across the air-sea interface, the temperature-dependent solubility of CO_2, and the difference between the prescribed pCO_2 of the atmosphere and the pCO_2 of the uppermost layer of the ocean (Doney et al., 2006). The ocean carbon cycle model predicts seven prognostic variables that are transported by the ocean model: phosphate (PO_4), total dissolved inorganic iron, dissolved organic phosphorus and iron, dissolved inorganic carbon, total alkalinity, and dissolved oxygen. The parameterization of biological uptake of nutrients is similar to that used in the Hamburg Model of the Ocean Carbon Cycle (HAMOCC; Maier-Reimer, 1993) and assumes a constant Redfield ratio (Redfield, 1958) for particulate organic matter. The uptake of PO_4 is given by the turnover of biomass, modulated by surface temperature, solar irradiance, and macro- and micronutrients. The model uses the Redfield ratio (Redfield, 1963) and the Martin power-law curve (Winguth and Winguth, 2013) to show the vertical flux of particulate organic phosphorus (F_{POP}) for the entire water column.

4.3 Boundary Conditions and Experimental Design

The concentration of the greenhouse gases is taken as 2.38 x $(10)^{-4}$ ppm for CO_2, 632 x $(10)^{-9}$ ppb for CH_4 and 265 x $(10)^{-9}$ ppb for N_2O from Joos et al. (2008) and the file for ozone concentration has been obtained from He, 2011. The Solar Constant is taken as 1.365 x $(10)^6$ W/m^2 (Otto-Bleisner et al., 2006) and the Orbital constant is -11,150. The atmospheric pCO_2 is transient (He, 2011 and Hughlett (pers. comm.)) and the ice mask used is Ice5G (Peltier, 2004). A Dynamic Global Vegetation Model as used by Liu et al., 2009 has been employed here. The aerosol optics and the absorption and emission parameters are taken from He, 2011.

Two simulations have been conducted; one will be for the Younger Dryas time period (approximately 13,100 years before present, or 13.1ka, PhD. Diagnostic Proposal,

Hughlett, 2012), and the other for present day climate conditions, based on a previous study by Yeager et al. (2006). Both simulations implement a dynamic global vegetation model (DGVM) that is built into CLM. The present day simulation branches out from Yeager et al. (2006) and has been integrated for 1500 years by Winguth et al. (2010). The Younger Dryas simulation branches from a transient simulation by He (2011) for the Last Glacial Maximum (LGM), and has been integrated for approximately 100 years (13,100 years before present by Hughlett, 2012). Each of the five components for CCSM3 required change to match the boundary conditions of the Younger Dryas, and all restart and boundary condition files were obtained from He, (2011). In POP, topography and the region mask were replaced.

Chapter 5

Temperature, Salinity and $\delta^{18}O$ Database

5.1 Present Day Temperature and Salinity

Temperature and salinity data utilized in this study are taken from the World Ocean Circulation Experiment (WOCE), a global oceanic hydrographic survey from 1990 to 1998 including the Antarctic, Atlantic, Indian and Pacific oceans and was aimed towards (a) providing data to develop models useful in climate change prediction and (b) forming a representative data set in order to study the long term behavior of the world oceans. WOCE temperature and salinity data were gathered for the present day and Younger Dryas $\delta^{18}O$ benthic carbonate data are latitudinal locations and zonally averaged (Latitude vs. Depth) in order to compare oxygen isotope distribution with those of the Younger Dryas.

5.2 Present Day and Younger Dryas $\delta^{18}O$

One objective of the current study was creating a $\delta^{18}O$ carbonate database for the present day and Younger Dryas to interpret how well the simulation with CCSM3 agree with the ocean structure. The online database of the National Climate Data Center (NCDC) (World Data Center for Paleoclimatology) and Pangaea (http://pangaea.de/) has been used in this stud. The paleoceanography reconstructions from there centers include proxies from deep sea sediments such as trace metal and isotopic composition of fossil plankton, species composition, and lithology. The Pangaea database is an online information system which operates as an open access library aimed at archiving, publishing and distributing geo-referenced data.

The compiled data of the Atlantic Ocean has a longitudinal extent of 100°W to 20°E ranging from the Gulf of Mexico in the east to the GIN Seas in the west and a latitudinal range from the Arctic to the Antarctic (90°N to 80°S). In order to get an

accurate understanding of the $\delta^{18}O$ distribution and how they are affected by freshwater input, $\delta^{18}O$ values inferred from benthic foraminifera are collected. The present day and Younger Dryas $\delta^{18}O$ databases by Labeyrie et al., 1992 (Table 1) and Sarnthein et al., 1994 (Table 2) are used for this study. Commonly occurring benthic foraminiferal species *Cibicides wuellerstorfi*, constitutes majority of both the compiled databases of present day and Younger Dryas and that of Labeyrie et al., 1992 and Shackleton et al., 1994.

Table 1 Location of cores (latitude, longitude, depth) where benthic foraminifera have been analyzed (Labeyrie et al., 1992). References for the isotopic analyses: (1) CFR-Gif; (2) Kiel: Winn et al., (1991); Zahn et al., (1986); (3) G.L. Cambridge.

Core	Latitude	Longitude	Depth	YD $\delta^{18}O$	PD $\delta^{18}O$	Ref
V 27-60	72.18	-08.58	2525	4.92	4.52	1
K 11	71.78	-01.60	2900	4.89	4.57	1
V 28-38	69.38	-04.40	3411	5.02	4.53	1
V 28-14	64.78	-29.56	1855	3.36	3.11	3
BOFS 17K	58.00	-16.50	1150	4.39	-	3
CH 73-139C	54.63	-16.53	2209	4.14	3.30	1
M 15-612	44.36	-26.55	3050	-	3.10	2
SU 81-44	44.25	-02.70	1173	3.99	2.45	1
V 29-179	44.00	-24.53	3331	-	3.33	3
SU 81-32	42.10	-09.78	2280	4.01	3.37	1
CH 69-09	41.75	-47.35	4100	4.24	3.42	1
SU 81-24	39.31	-10.53	2239	4.21	3.19	1
SU 81-21	38.25	-09.55	1260	-	2.07	1
SU 81-18	37.76	-10.18	3135	3.97	3.45	1
M 15-669	34.90	-07.81	2022	-	3.10	2
M 15-672	34.86	-08.13	2455	-	3.14	2
NO 78-07	34.33	-07.01	0700	2.99	2.07	1
M 16-004	29.98	-10.65	1512	-	2.84	2
M 16-006	29.25	-11.50	0796	-	2.24	2
M 12-309	26.83	-15.11	2820	4.10	3.24	2
M 12-392	25.16	-16.83	2573	3.75	3.21	2
M 12-379	23.13	-17.75	2136	4.14	3.14	2
M 16-030	21.23	-18.13	1500	-	3.15	2
M 12-328	21.15	-18.56	2778	4.23	3.38	2
M 13-289	18.06	-18.01	2490	4.26	3.30	2
M 12-347	15.83	-17.86	2576	4.09	3.36	2
V 22-197	14.16	-18.58	3167	-	3.17	3
V 22-196	13.83	-18.96	3728	-	3.20	3
M 13-519	05.66	-19.85	2862	-	3.29	2

Table 1 — *Continued*

KW-31	03.18	05.56	1515	3.79	3.00	1
V 25-59	01.36	-33.48	3824	-	3.20	3

Specific fractionation corrections have been employed by Labeyrie et al. to all $\delta^{18}O$ analyses using the following additive factors: +0.64‰ for *Cibicides wuellerstorfi*, +0.4‰ for *Melonis* and no corrections for the different *Uvigerina* species (Shackleton and Opdyke, 1973; Duplessy et al., 1984).

A similar benthic stable isotope database (Table 2, Sarnthein et al., 1994) of nearly 95 core locations exists published and unpublished sources. The sources are as listed in Table 3. Sarnthein et al. (1994) compiled eight time slices for the most recent 30,000 years to reproduce the evolution of the Atlantic deepwater oceanography. Characteristics such as sedimentation, climatic fluctuations, abrupt climate change and response to climatic changes were used as guiding factors to determine each time interval. As per the requirement of the current study, isotope data from intervals pertaining only to present day (Time slice (1), 0-4000 cal years ago) and Younger Dryas (Time slice (4), 11,800/12,300-12,800 cal years ago) are listed in Table 2.

Table 2 Location of cores (latitude, longitude, depth) where benthic foraminifera have been analyzed (Sarnthein et al., 1994).

Core	Lat	Long	Depth	YD $\delta^{18}O$	PD $\delta^{18}O$	Ref
V 28-14	64.78	-29.56	1855	-	3.51	k
V 29-198	59.00	-19.00	1139	1.76	-	t
V 28-73	57.00	-20.00	2063	-	3.11	t
17051	56.16	-31.99	2295	2.68	-	a
DSDP 552	56.05	-23.23	2311	-	3.66	r
NA 87-22	55.50	-14.70	2161	2.56	3.42	b
17050	55.47	-27.89	2795	2.59	-	a
17049	55.26	-26.73	3331	2.64	3.30	a
V 29-193	55.00	-19.00	1326	2.39	3.40	t
23419	54.96	-19.76	1491	-	3.02	a
CH 73-139c	54.63	-16.35	2209	3.00	-	b
17048	54.31	-18.18	1859	2.50	3.18	b
V 23-81	54.25	-16.83	2393	2.70	3.53	n
23414	53.54	-20.29	2196	2.91	3.43	a

Table 2 — *Continued*

17045	52.43	-16.66	3663	2.59	-	a
17054	48.45	-27.70	1834	2.73	3.38	a
17055	48.22	27.06	2558	2.51	3.16	a
17056	48.04	-25.09	3599	2.77	-	a
SU 81-50	45.38	-04.65	4320	3.68	-	b
15612	44.69	-26.54	3050	2.42	3.37	a
SU 81-44	44.25	-02.70	1173	-	3.46	b
CH 82-50-20	43.50	-29.87	3020	-	3.12	h
CH 82-41-15	43.37	-28.23	2151	-	3.37	h
SU 81-32	42.10	-09.78	2280	-	3.90	b
CH 72-02	40.60	-21.70	3485	2.68	3.50	b
SU 92-21	36.57	-23.74	4170	-	3.27	a
11944	35.65	-08.06	1765	2.19	3.02	a
15666	34.96	-07.12	0803	1.59	2.20	a,w
15670	34.91	-07.85	1482	-	3.00	a
15669	34.89	-07.81	2001	2.43	2.92	a
15672	34.86	-08.13	2435	2.31	3.20	a
T 86-15P	30.43	-37.07	3375	-	3.67	f
16004	29.98	-10.65	1512	2.13	2.76	a
16006	29.27	-11.50	0796	1.70	-	a,w
15637	27.01	-18.99	3849	-	3.67	a
12309	26.84	-15.11	1280	2.60	3.29	a
12392	25.17	-16.85	2575	2.50	3.50	a,s
12310	23.50	-18.72	3080	2.44	3.30	a
12379	23.14	-17.75	2136	2.64	3.12	a
V 23-100	21.30	-21.68	4579	2.43	-	e
16017	21.25	-17.80	0812	1.38	3.10	a
16030	21.24	-18.06	1500	2.47	3.08	a
12328	21.15	-18.57	2778	2.72	3.60	a
ODP 658	20.75	-18.58	2263	2.74	3.52	a
12329	19.37	-19.93	3314	2.50	2.92	a
ODP 659	18.08	-21.03	3069	2.38	-	a
13289	18.07	-18.01	2490	2.63	2.97	a
ALB 226	17.95	-21.05	3100	2.62	3.28	d
12337	15.95	-18.13	3088	2.60	3.57	a
12347	15.83	-17.86	2576	2.60	3.43	a
12345	15.48	-17.36	0945	2.37	-	a
16402	14.42	-20.57	4230	2.62	3.57	a
V 22-197	14.16	-18.58	3167	-	3.67	k
V 22-196	13.83	-18.97	3728	-	3.62	g
16415	09.57	-19.11	3841	2.67	3.38	a
16407	09.04	-21.96	4596	2.73	-	a
16408	09.01	-21.50	4336	2.67	2.84	a
16459	07.28	-26.19	4835	2.47	3.36	a
13519	05.66	-19.85	2862	2.80	3.48	a
ENO 66-16	05.46	-21.14	3152	-	3.31	j
16457	05.39	-21.72	3291	2.68	3.19	a

Table 2 — *Continued*

16458	05.34	-22.06	3518	3.07	3.43	a
16455	05.27	-22.87	4160	2.61	3.42	a
ENO 66-38	04.92	-20.50	2931	-	3.00	j
16453	04.73	-20.95	2675	2.79	3.08	a
ENO 66-21	04.23	-21.63	3995	-	3.07	j
ENO 66-26	03.09	-20.02	4745	-	3.00	j
13521	03.02	-22.03	4504	-	3.20	a
ENO 66-32	02.47	-19.73	5003	-	3.70	j
ENO 66-29	02.46	-19.76	5104	-	3.50	j
V 25-59	01.37	-33.48	3824	2.57	3.50	o
V 30-40	-00.20	-23.15	3706	-	3.02	q
16773	-00.97	-09.44	4662	2.60	3.80	a
16772	-01.21	-11.96	3912	2.40	-	a
16867	-02.20	05.10	3891	2.60	3.10	a
BT 4	-04.33	10.43	1000	-	2.99	k
MG-237	-05.20	11.33	1000	2.72	3.58	b
Geo B-1113	-05.75	-11.04	2374	2.71	3.40	a
V 29-135	-19.60	08.88	2675	2.60	3.32	a,c
RC 13-228	-22.33	11.20	3204	2.55	-	k
RC 13-229	-25.50	11.30	4194	-	3.05	k
RC 11- 83	-41.60	09.72	4718	-	2.90	i

Table 3 List of referenced sources of isotope database for Sarnthein et al. 1994

a	University of Kiel (published and unpublished)
b	Centre des Faibles Radioactivitès, laboratoire mixte CNRS-CEA, Gif-sur Yvette Cedex, France. (published and unpublished)
c	Abrantes (unpublished data, 1993)
d	Bornmalm (unpublished data, 1993)
e	Fairbanks (unpublished data, 1992)
f	Ganssen (unpublished data, 1992)
g	Shackleton (unpublished data, 1992)
h	Boyle and Keigwon [1985,1987]
i	Charles and Fairbanks [1992]
j	Curry and Lohmann [1985]
k	Curry et al. [1984]
n	Jansen and Veum [1990]
o	Mix and Ruddiman [1985]
q	Oppo and Lehman [1993]
r	Shackleton and Hall [1984]
s	Shackleton [1977]
w	C. *wuellerstorfi* and P. *ariminensis*

It should be noted that for the online databases, a simple averaging technique has been employed for $\delta^{18}O$ values belonging to the Younger Dryas period (11,900 ka –

10,500 ka years ago) owing to a non-uniform age distribution across the different core datasets. Many online databases have $\delta^{18}O$ information from a variety of foraminifer species, in which case the representative benthic species (*Cibicides wuellerstorfi*) has been considered.

Chapter 6

Error Analysis

The purpose of this chapter is to quantify errors related to the paleoclimate data and CCSM3. Two major data sets consist of 87 present day and 86 Younger Dryas benthic stable oxygen isotope data points (cores) from Labeyrie et al., 1992 (Table 1) and Sarnthein et al., 1994 (Table 2). In addition, 131 Younger Dryas data points from various articles have been gathered through NCDC and the Pangaea online databases, a list of which can be found in Table 8.

Errors will be discussed in the following:

6.1 Error Related to CCSM3

The performance of CCSM3 in the computationally efficient configuration is discussed by Yeager et al. (1996). This coarse resolution model generally represents the mean climate but does not resolve mountain ranges or ocean shelves. This model shows a double ITCZ problem, wherein a false Inter-Tropical Convergence Zone appears south of equator in the central and eastern equatorial Pacific apart from the observed one north of the equator (Zhang and Wang, 2006). The ENSO variability is not adequately produced (Yeager, 2006). In addition, this model shows discrepancy in the outgoing longwave radiation and absorbed solar radiation due to a bias in the cloud forcing distribution (Yeager, 2006). The T31x1 simulates a too weak Atlantic heat transport, displaced Southern Hemisphere storm tracks and a less dynamic THC due to feeble deep water formation. Most of these errors are of complex nature.

6.2 Temperature and Salinity Data Error in Model and Observations

There are various factors influencing the errors in climate model as has been discussed in section 6.1. As a result, climate models lead to an error in the output and it

is desirable to recognize, quantify and eliminate the error sources in order to improve accuracy of the climate prediction.

For any given parameter "X" in a climate model, it is accurate to say that,

$$\mathrm{X_{model}} = \mathrm{X_{obs}} + \mathrm{X_{error}} \tag{6-1}$$

Hence,

$$\mathrm{X_{error}} = \mathrm{X_{model}} - \mathrm{X_{obs}} \tag{6-2}$$

Where X_{model} is the value of parameter X as seen in the model output, X_{obs} is the physically measured value of parameter X taken from either of the data sets and X_{error} is the error in the model.

In the following, errors affecting the predicted δ_c ($\delta^{18}O$ from benthic foraminifers / carbonates) are discussed. As seen in equation (2-1), δ_w (SMOW) is directly proportional to salinity and in equation (2-3), δ_c depends on δ_w and temperature. For simplicity, errors for temperature, salinity and δ_c from the previously mentioned databases are described first for present day and only δ_c for Younger Dryas.

6.2.1 Present Day

Using equation (6-2), we can describe the error in temperature and salinity as follows:

$$\mathrm{T_{error}} = \mathrm{T_{model}} - \mathrm{T_{obs}} \tag{6-3}$$

$$\mathrm{S_{error}} = \mathrm{S_{model}} - \mathrm{S_{obs}} \tag{6-4}$$

Here, we use the corresponding observed temperature and salinity values from the WOCE and compare the estimated δ_c from WOCE with the predicted δ_c from CCSM3 and

observed values inferred from benthic foraminifera (Labeyrie et al., 1992 and Sarnthein et al., 1994) using equation (6-3) and (6-4) in Table 4 and Table 5.

For the data points corresponding to Labeyrie et al., the average error for the present day temperature values for the model is -1.11℃ compared to WOCE which is nearly double compares to 0.77℃ of Sarnthein et al. (1994). The mean temperatures, 2.65℃ and 2.45℃, for the model corresponding to both databases is around 1℃ less than the corresponding WOCE temperature of 3.76℃ and 3.22℃. The maximum and minimum errors for Labeyrie et al. (1992) are -2.75℃ and -0.05℃ respectively which are again considerably higher than -0.35 and 0.25℃ of Sarnthein et al.(1994). For both the databases, error values do not exhibit any particular trend from North to South Atlantic and their change with depth is uneven. The model shows an overall lower value for temperature compared to WOCE.

The corresponding mean salinity for Labeyrie et al. (1992) is 34.79 psu which is nearly the same as that of Sarnthein et al (1994) at 34.75 psu. Both are also very close to their respective WOCE values, 35.04 and 34.50 and almost the same as the mean global salinity 34.74 ‰ (Östlund et al., 1987). The average error in salinity for Labeyrie et al. (1992) and Sarnthein et al. (1994) are -0.24 psu and -0.22 psu respectively. As seen in equation (2-3), salinity does not significantly impact δ_c due to the nature of the formula. The model salinity again shows an overall lower value compared WOCE.

In case of δc, the model shows a higher fidelity to the WOCE database rather than Labeyrie et al. (1992) or Sarnthein et al. (1994), the average error being a very low 0.20 ‰ compared to WOCE. Although, in terms of latitude, there's no particular trend in the error for the model values compared to WOCE and observed in either of the databases, a considerable agreement is seen in the tropical Atlantic region.

Table 4 Error analysis for Present Day δ_c of cores where benthic foraminifera have been analyzed (Labeyrie et al., 1992)

	Core	Depth	Lat	Long	δ_c (Obs)	δ_c (WOCE)	δ_c (CCSM3)	Error δ_c (CCSM3 vs. Obs)	Error δ_c (CCSM3 vs. WOCE)	T (CCSM3)	T (WOCE)	S (CCSM3)	S (WOCE)	δ_w (SMOW)
1	V27-60	2525	72.18	-08.58	4.52	4.11	4.6	0.08	0.49	1.25	2.80	34.70	34.98	0.30
2	K11	2900	71.78	-01.60	4.57	4.19	4.6	0.03	0.41	1.25	2.50	34.70	34.95	0.29
3	V28-38	3411	69.38	-04.40	4.53	4.26	4.6	0.07	0.34	1.25	2.20	34.70	34.91	0.27
4	V 28-14	1855	64.78	-29.56	3.11	3.89	4.2	1.09	0.31	1.25	3.50	34.70	34.98	0.30
5	CH 73-139C	2209	54.63	-16.35	3.30	4.06	4.2	0.90	0.14	2.75	2.90	34.90	34.95	0.29
6	M 15-612	3050	44.36	-26.55	3.10	4.15	4.2	1.10	0.05	1.25	2.60	34.70	34.95	0.29
7	SU 81-44	1173	44.25	-02.70	2.45	3.08	3.4	0.95	0.32	4.25	6.80	34.90	35.30	0.47
8	V 29-179	3331	44.00	-24.53	3.33	4.21	4.4	1.07	0.19	1.25	2.40	34.70	34.93	0.28
9	SU 81-32	2280	42.10	-09.78	3.37	3.98	4.0	0.63	0.02	2.75	3.20	34.90	34.98	0.30
10	CH 69-09	4100	41.75	-47.35	3.42	4.26	4.6	1.18	0.34	1.25	2.20	34.70	34.91	0.27
11	SU 81-24	2239	39.31	-10.53	3.19	3.91	3.8	0.61	-0.11	2.75	3.50	34.90	35.01	0.32
12	SU 81-12	1260	38.25	-09.55	2.07	3.04	3.4	1.33	0.36	5.75	7.50	35.10	35.60	0.62
13	SU 81-18	3135	37.76	-10.18	3.45	4.18	4.2	0.75	0.02	1.25	2.50	34.70	34.94	0.28
14	M 15-669	2022	34.90	-07.81	3.10	3.86	3.8	0.70	-0.06	2.75	3.70	34.70	35.04	0.33
15	M 15-672	2455	34.86	-08.13	3.14	4.04	4.2	1.06	0.16	2.75	3.00	34.90	34.97	0.30
16	NO 78-07	0700	34.33	-07.01	2.07	2.28	2.6	0.53	0.32	7.25	10.00	35.50	35.45	0.55
17	M 16-004	1512	29.98	-10.65	2.84	3.34	3.8	0.96	0.46	4.25	5.90	34.90	35.30	0.47
18	M 16-006	0796	29.25	-11.50	2.24	2.34	2.6	0.36	0.26	7.25	9.80	35.00	35.45	0.55
19	M 12-309	2820	26.83	-15.11	3.24	4.15	4.2	0.96	0.05	2.00	2.60	34.70	34.95	0.29
20	M 12-392	2573	25.16	-16.83	3.21	4.07	4.2	0.99	0.13	2.75	2.90	34.70	34.97	0.30
21	M 12-379	2136	23.13	-17.75	3.14	3.91	4.0	0.86	0.09	2.75	3.50	34.70	35.02	0.32
22	M 16-030	1500	21.23	-18.13	3.15	3.57	3.8	0.65	0.23	4.25	4.70	34.80	35.06	0.34
23	M 12-328	2778	21.15	-18.56	3.38	4.15	4.2	0.82	0.05	1.25	2.60	34.70	34.95	0.29
24	M 13-289	2490	18.06	-18.01	3.30	4.07	4.2	0.90	0.13	2.75	2.90	34.70	34.96	0.29
25	M 12-347	2576	15.83	-17.86	3.36	4.09	4.2	0.84	0.11	2.75	2.80	34.70	34.95	0.29
26	V 22-197	3167	14.16	-18.58	3.17	4.20	4.4	1.23	0.20	1.25	2.40	34.70	34.92	0.27

Table 4 — *Continued*

27	V 22-196	3728	13.83	-18.96	3.20	4.29	4.6	1.40	0.31	1.25	2.10	34.70	34.90	0.26
28	M 13-519	2862	05.66	-19.85	3.29	4.17	4.2	0.91	0.03	1.25	2.50	34.70	34.93	0.28
29	KW-31	1515	03.18	05.56	3.00	3.52	3.8	0.80	0.28	3.50	4.70	34.70	34.96	0.29
30	V 25-59	3824	01.36	-33.48	3.20	4.28	4.6	1.40	0.32	1.25	2.10	34.70	34.89	0.25

Table 5 Error analysis for Present Day δ_c of cores where benthic foraminifera have been analyzed (Sarnthein et al., 1994)

	Core	Depth	Lat	Long	δ_c (Obs)	δ_c (WOCE)	δ_c (CCSM3)	Error δ_c (CCSM3 vs. Obs)	Error δ_c (CCSM3 vs. WOCE)	T (CCSM3)	T (WOCE)	S (CCSM3)	S (WOCE)	δ_w (SMOW)
1	V 29-198	1139	59.00	-19.00	1.76	3.4	3.60	1.64	-0.20	4.25	4.4	34.90	34.94	0.28
2	17051	2295	56.16	-31.99	2.68	4.2	4.06	1.52	0.14	2.75	2.9	34.90	34.95	0.29
3	NA 87-22	2161	55.50	-14.70	2.56	4.0	4.03	1.44	-0.03	2.75	3.0	34.90	34.95	0.29
4	17050	2795	55.47	-27.89	2.59	4.2	4.08	1.61	0.12	2.75	2.8	34.80	34.93	0.28
5	17049	3331	55.26	-26.73	2.64	4.6	4.17	1.96	0.43	1.25	2.5	34.90	34.93	0.28
6	V 29-193	1326	55.00	-19.00	2.39	3.8	3.74	1.41	0.06	4.25	4.0	34.90	34.98	0.30
7	CH 73-1396	2209	54.63	-16.35	3.00	4.2	4.04	1.20	0.16	2.75	3.0	34.90	34.97	0.30
8	17048	1859	54.31	-18.18	2.50	3.8	3.90	1.30	-0.10	2.75	3.4	34.90	34.94	0.28
9	V 23-81	2393	54.25	-16.83	2.70	4.2	4.09	1.50	0.11	2.75	2.8	34.90	34.95	0.29
10	23414	2196	53.54	-20.29	2.91	4.2	4.03	1.29	0.17	2.75	3.0	34.90	34.95	0.29
11	17045	3663	52.43	-16.66	2.59	4.6	4.26	2.01	0.34	1.25	2.2	34.70	34.91	0.27
12	17054	1834	48.45	-27.70	2.73	3.8	3.86	1.07	-0.06	2.75	3.5	34.90	34.92	0.27
13	17055	2558	48.22	27.06	2.51	4.2	4.03	1.69	0.17	2.75	3.0	34.70	34.96	0.29
14	17056	3599	48.04	-25.09	2.77	4.6	4.23	1.83	0.37	1.25	2.3	34.70	34.91	0.27
15	SU 81-50	4320	45.38	-04.65	3.68	4.6	4.26	0.92	0.34	1.25	2.2	34.70	34.91	0.27
16	15612	3050	44.69	-26.54	2.42	4.2	4.15	1.78	0.05	1.25	2.6	34.70	34.95	0.29
17	CH 72-02	3485	40.60	-21.70	2.68	4.6	4.26	1.92	0.34	1.25	2.2	34.70	34.91	0.27
18	11944	1765	35.65	-08.06	2.19	4.2	3.36	2.01	0.84	4.25	5.7	34.90	35.20	0.42
19	15666	0803	34.96	-07.12	1.59	3.0	2.53	1.41	0.47	6.50	9.5	34.30	35.67	0.66
20	15669	2001	34.89	-07.81	2.43	3.8	3.83	1.37	-0.03	2.75	3.8	34.90	35.04	0.33
21	15672	2435	34.86	-08.13	2.31	4.2	4.04	1.89	0.16	2.75	3.0	34.90	34.98	0.30

Table 5 — *Continued*

22	16004	1512	29.98	-10.65	2.13	3.8	3.46	1.67	0.34	4.25	5.5	34.90	35.30	0.47
23	16006	0796	29.27	-11.50	1.70	2.6	2.18	0.90	0.42	8.75	10.5	34.50	35.50	0.57
24	12309	2820	26.84	-15.11	2.60	3.4	3.02	0.80	0.38	4.25	7.3	34.90	35.45	0.55
25	12392	2575	25.17	-16.85	2.50	4.2	4.09	1.70	0.11	2.75	2.9	34.70	34.97	0.30
26	12310	3080	23.50	-18.72	2.44	4.2	4.21	1.76	-0.01	1.25	2.4	34.70	34.93	0.28
27	12379	2136	23.14	-17.75	2.64	4.0	3.91	1.36	0.09	2.75	3.5	34.70	35.02	0.32
28	V 23-100	4579	21.30	-21.68	2.43	4.6	4.34	2.17	0.26	1.25	1.9	34.70	34.88	0.25
29	16017	0812	21.25	-17.80	1.38	3.6	2.81	2.22	0.79	7.25	7.3	34.90	35.04	0.33
30	16030	1500	21.24	-18.06	2.47	3.8	3.57	1.33	0.23	4.25	4.7	34.90	35.06	0.34
31	12328	2778	21.15	-18.57	2.72	4.2	4.14	1.48	0.06	1.25	2.6	34.70	34.95	0.29
32	ODP 658	2263	20.75	-18.58	2.74	4.2	3.99	1.46	0.21	2.75	3.2	34.70	34.99	0.31
33	12329	3314	19.37	-19.93	2.50	4.6	4.21	2.10	0.39	1.25	2.4	34.70	34.92	0.27
34	ODP 659	3069	18.08	-21.03	2.38	4.2	4.21	1.82	-0.01	1.25	2.4	34.70	34.93	0.28
35	13289	2490	18.07	-18.01	2.63	4.2	4.06	1.57	0.14	2.75	2.9	34.70	34.95	0.29
36	ALB 226	3100	17.95	-21.05	2.62	4.2	4.21	1.58	-0.01	1.25	2.4	34.70	34.93	0.28
37	12337	3088	15.95	-18.13	2.60	4.2	4.22	1.60	-0.02	1.25	2.4	34.70	34.93	0.28
38	12347	2576	15.83	-17.86	2.60	4.2	4.09	1.60	0.11	2.75	2.8	34.70	34.95	0.29
39	12345	0945	15.48	-17.36	2.37	3.4	3.10	1.03	0.30	5.75	6.0	34.70	34.89	0.25
40	16402	4230	14.42	-20.57	2.62	4.6	4.31	1.98	0.29	1.25	2.0	34.70	34.89	0.25
41	16415	3841	09.57	-19.11	2.67	4.6	4.29	1.93	0.31	1.25	2.1	34.70	34.90	0.26
42	16407	4596	09.04	-21.96	2.73	4.6	4.34	1.87	0.26	1.25	1.9	34.70	34.88	0.25
43	16408	4336	09.01	-21.50	2.67	4.6	4.31	1.93	0.29	1.25	2.0	34.70	34.88	0.25
44	16459	4835	07.28	-26.19	2.47	4.6	4.27	2.13	0.33	1.25	2.1	34.70	34.87	0.24
45	13519	2862	05.66	-19.85	2.80	4.2	4.17	1.40	0.03	1.25	2.5	34.70	34.92	0.27
46	16457	3291	05.39	-21.72	2.68	4.6	4.23	1.92	0.37	1.25	2.3	34.70	34.91	0.27
47	16458	3518	05.34	-22.06	3.07	4.6	4.25	1.53	0.35	1.25	2.2	34.70	34.90	0.26
48	16455	4160	05.27	-22.87	2.61	4.6	4.31	1.99	0.29	1.25	2.0	34.70	34.89	0.25
49	16453	2675	04.73	-20.95	2.79	4.2	4.14	1.41	0.06	1.25	2.6	34.70	34.93	0.28
50	V 25-59	3824	01.37	-33.48	2.57	4.6	4.28	2.03	0.32	1.25	2.1	34.70	34.89	0.25
51	16773	4662	-00.97	-09.44	2.60	4.6	4.74	2.00	-0.14	0.50	0.4	34.70	34.72	0.17
52	16772	3912	-01.21	-11.96	2.40	4.6	4.34	2.20	0.26	1.25	1.9	34.70	34.89	0.25
53	16867	3891	-02.20	05.10	2.60	4.6	4.37	2.00	0.23	1.25	1.8	34.70	34.88	0.25

Table 5 — *Continued*

54	MG-237	1000	-05.20	11.33	2.72	3.4	3.61	0.68	-0.21	4.25	4.1	34.70	34.80	0.21
55	Geo B-1113	2374	-05.75	-11.04	2.71	4.2	4.09	1.49	0.11	2.75	2.8	34.70	34.93	0.28
56	V 29-135	2675	-19.60	08.88	2.60	4.2	4.14	1.60	0.06	1.25	2.6	34.70	34.92	0.27
57	RC 13-228	3204	-22.33	11.20	2.55	4.6	4.23	2.05	0.37	1.25	2.3	34.70	34.91	0.27

6.2.2. Younger Dryas

Table 6,Table 7 and Table 8 show the Younger Dryas δ_c error analysis for Labeyrie et al., 1992, Sarnthein et al., 1994 and data collected from NCDC and Pangaea online databases respectively. Out of the three, Labeyrie et al. (1992) data shows the most agreement with the model values showing an error of only 1.04 ‰ whereas Sarnthein et al., NCDC and Pangaea databases show almost twice the error, 2.31 ‰ and 2.04 ‰ respectively. If we neglect a few data points, all the databases show an increase in error with respect to depth. There is no particular trend seen from North to South in any of the databases. The North tropical and equatorial Atlantic show a consistently high amount of error (>2 ‰) for the Sarnthein et al. (1994) database.

Table 6 Error analysis for Younger Dryas δ_c of cores where benthic foraminifera have been analyzed (Labeyrie et al., 1992)

	Core	Depth	Lat	Long	δ_c (Obs)	δ_c (CCSM3)	Error δ_c (CCSM3 vs. Obs)
1	V27-60	2525	72.18	-08.58	4.92	5.25	0.33
2	K11	2900	71.78	-01.60	4.89	5.25	0.36
3	V28-38	3411	69.38	-04.40	5.02	4.95	-0.07
4	V 28-14	1855	64.78	-29.56	3.36	5.25	1.89
5	BOFS 17K	1150	58.00	-16.50	4.39	4.65	0.26
6	CH 73-139C	2209	54.63	-16.35	4.14	5.25	1.11
7	SU 81-44	1173	44.25	-02.70	3.99	4.65	0.66
8	SU 81-32	2280	42.10	-09.78	4.01	5.25	1.24
9	CH 69-09	4100	41.75	-47.35	4.24	5.85	1.61
10	SU 81-24	2239	39.31	-10.53	4.21	5.25	1.04
11	SU 81-18	3135	37.76	-10.18	3.97	5.55	1.58
12	NO 78-07	0700	34.33	-07.01	2.99	4.05	1.06
13	M 12-309	2820	26.83	-15.11	4.10	5.25	1.15
14	M 12-392	2573	25.16	-16.83	3.75	5.55	1.80
15	M 12-379	2136	23.13	-17.75	4.14	5.25	1.11
16	M 12-328	2778	21.15	-18.56	4.23	5.55	1.32
17	M 13-289	2490	18.06	-18.01	4.26	5.25	0.99
18	M 12-347	2576	15.83	-17.86	4.09	5.55	1.46
19	KW-31	1515	03.18	05.56	3.79	4.65	0.86

Table 7 Error analysis for Younger Dryas δ_c of cores where benthic foraminifera have been analyzed (Sarnthein et al., 1994)

	Core	Depth	Lat	Long	δ_c (Obs)	δ_c (CCSM3)	Error δ_c (CCSM3 vs. Obs)
1	V 28-14	1855	64.78	-29.56	3.51	5.25	1.74
2	V 28-73	2063	57.00	-20.00	3.11	5.25	2.14
3	DSDP 552	2311	56.05	-23.23	3.66	5.55	1.89
4	NA 87-22	2161	55.50	-14.70	3.42	5.25	1.83
5	17049	3331	55.26	-26.73	3.30	5.55	2.25
6	V 29-193	1326	55.00	-19.00	3.40	4.95	1.55
7	23419	1491	54.96	-19.76	3.02	4.95	1.93
8	17048	1859	54.31	-18.18	3.18	5.25	2.07
9	V 23-81	2393	54.25	-16.83	3.53	5.55	2.02
10	23414	2196	53.54	-20.29	3.43	5.25	1.82
11	17054	1834	48.45	-27.70	3.38	5.25	1.87
12	17055	2558	48.22	27.06	3.16	5.55	2.39
13	15612	3050	44.69	-26.54	3.37	5.55	2.18
14	SU 81-44	1173	44.25	-02.70	3.46	4.65	1.19
15	CH 82-50-20	3020	43.50	-29.87	3.12	5.55	2.43
16	CH 82-41-15	2151	43.37	-28.23	3.37	5.25	1.88
17	SU 81.32	2280	42.10	-09.78	3.90	5.25	1.35
18	CH 72-02	3485	40.60	-21.70	3.50	5.55	2.05
19	SU 92-21	4170	36.57	-23.74	3.27	5.85	2.58
20	11944	1765	35.65	-08.06	3.02	4.95	1.93
21	15666	0803	34.96	-07.12	2.20	4.35	2.15
22	15670	1482	34.91	-07.85	3.00	4.65	1.65
23	15669	2001	34.89	-07.81	2.92	5.25	2.33
24	15672	2435	34.86	-08.13	3.20	5.25	2.05
25	T 86-15P	3375	30.43	-37.07	3.67	5.25	1.58
26	16004	1512	29.98	-10.65	2.76	4.65	1.89
27	15637	3849	27.01	-18.99	3.67	5.85	2.18
28	12309	2820	26.84	-15.11	3.29	4.65	1.36
29	12392	2575	25.17	-16.85	3.50	5.25	1.75
30	12310	3080	23.50	-18.72	3.30	5.55	2.25
31	12379	2136	23.14	-17.75	3.12	5.25	2.13
32	16017	0812	21.25	-17.80	3.10	3.75	0.65
33	16030	1500	21.24	-18.06	3.08	4.65	1.57
34	12328	2778	21.15	-18.57	3.60	5.55	1.95
35	ODP 658	2263	20.75	-18.58	3.52	5.25	1.73
36	12329	3314	19.37	-19.93	2.92	5.55	2.63
37	13289	2490	18.07	-18.01	2.97	4.65	1.68
38	ALB 226	3100	17.95	-21.05	3.28	5.55	2.27
39	12337	3088	15.95	-18.13	3.57	5.55	1.98

Table 7 — *Continued*

40	12347	2576	15.83	-17.86	3.43	4.95	1.52
41	16402	4230	14.42	-20.57	3.57	5.85	2.28
42	V 22-197	3167	14.16	-18.58	3.67	5.55	1.88
43	V 22-196	3728	13.83	-18.97	3.62	5.85	2.23
44	16415	3841	09.57	-19.11	3.38	5.85	2.47
45	16408	4336	09.01	-21.50	2.84	5.85	3.01
46	16459	4835	07.28	-26.19	3.36	5.85	2.49
47	13519	2862	05.66	-19.85	3.48	5.55	2.07
48	ENO 66-16	3152	05.46	-21.14	3.31	5.55	2.24
49	16457	3291	05.39	-21.72	3.19	5.25	2.06
50	16458	3518	05.34	-22.06	3.43	5.85	2.42
51	16455	4160	05.27	-22.87	3.42	5.85	2.43
52	ENO 66-38	2931	04.92	-20.50	3.00	5.55	2.55
53	16453	2675	04.73	-20.95	3.08	5.55	2.47
54	ENO 66-21	3995	04.23	-21.63	3.07	5.85	2.78
55	ENO 66-26	4745	03.09	-20.02	3.00	5.85	2.85
56	13521	4504	03.02	-22.03	3.20	5.85	2.65
57	ENO 66-32	5003	02.47	-19.73	3.70	5.85	2.15
58	ENO 66-29	5104	02.46	-19.76	3.50	5.85	2.35
59	V 25-59	3824	01.37	-33.48	3.50	5.85	2.35
60	V 30-40	3706	-00.20	-23.15	3.02	5.85	2.83
61	16773	4662	-00.97	-09.44	3.80	5.85	2.05
62	16867	3891	-02.20	05.10	3.10	5.85	2.75
63	BT 4	1000	-04.33	10.43	2.99	4.35	1.36
64	MG-237	1000	-05.20	11.33	3.58	4.35	0.77
65	Geo B-1113	2374	-05.75	-11.04	3.40	5.25	1.85
66	V 29-135	2675	-19.60	08.88	3.32	5.55	2.23
67	RC 13-229	4194	-25.50	11.30	3.05	5.85	2.80

Table 8 Error analysis for Younger Dryas δ_c of cores where benthic foraminifera have been analyzed (Pangaea and NCDC online databases)

	Core	Depth	Lat	Long	δ_c (Obs)	δ_c (CCSM3)	Error δ_c (CCSM3 vs. Obs)
1	PS2138-1	0862	81.53	30.87	4.29	5.25	0.96
2	HUD91/039-012P	0823	76.80	-71.85	2.95	5.25	2.30
3	HM94-34	3004	73.76	-02.53	4.33	5.25	0.92
4	HM71-19	2210	69.48	-09.51	3.94	5.25	1.31
5	PS62/015-3	1013	67.93	-25.42	3.45	5.25	1.80
6	GIK23519-5	1893	64.79	-29.59	3.38	5.25	1.87
7	HM52-43	2781	63.51	-00.73	3.85	5.55	1.70
8	ODP984C	1648	61.42	-24.08	3.50	4.95	1.45
9	162-980	2180	55.48	-14.70	3.15	5.25	2.10
10	GIK17048-3	1859	54.30	-18.17	3.14	5.25	2.11
11	GIK17045-2	3663	52.43	-16.66	2.97	5.55	2.58
12	DSDP site 609	3884	49.88	24.23	3.72	5.85	2.13

Table 8 — *Continued*

13	GIK17055-1	2810	48.21	-27.05	3.15	5.55	2.40
14	V17-179	0455	46.51	-58.07	3.07	4.05	0.98
15	GIK15612-2	3050	44.36	-26.54	3.23	5.55	2.32
16	V17-178	4066	43.48	-54.86	2.49	5.85	3.36
17	HU73-011-1	1814	43.21	-60.41	3.13	4.95	1.82
18	HU72-021-3	2470	42.97	-59.91	3.19	5.25	2.06
19	HU73-031-7	4055	42.97	-55.24	3.06	5.85	2.79
20	AC85-4	0662	41.75	11.76	3.91	4.05	0.14
21	MD952042	3146	37.81	-10.17	3.84	5.55	1.71
22	KC82-21	0586	36.88	-07.65	2.65	4.05	1.40
23	KC82-26	0583	36.79	-07.81	2.82	4.05	1.23
24	KS82-30	0795	36.45	-03.89	2.98	4.35	1.37
25	KS82-31	0854	36.15	-03.26	3.66	4.35	0.69
26	MD95-2043	1841	36.14	-02.62	3.33	4.95	1.62
27	RC09-203	1287	36.13	-01.96	3.98	4.65	0.67
28	V26-176	3942	36.05	-72.38	3.36	5.85	2.49
29	SU92-21	4170	36.00	-23.50	3.18	5.85	2.67
30	MD99-2339	1177	35.88	-07.52	3.20	4.65	1.45
31	CH74-227	3225	35.26	-29.25	3.84	5.55	1.71
32	GIK15672-1	2460	34.86	-08.12	3.17	5.25	2.08
33	GIK16004-1	1512	29.97	-10.64	2.87	4.65	1.78
34	22GGC2012	3924	29.78	43.58	3.99	5.85	1.86
35	GIK16006-1	0796	29.24	-11.49	3.02	4.05	1.03
36	GeoB4223-2	0775	29.01	-12.46	2.94	3.75	0.81
37	MD02-2575	0847	29.00	-87.11	3.68	3.85	0.17
38	GeoB4240-2	1358	28.88	-13.22	2.50	4.65	2.15
39	GIK15637-1	3849	27.00	-18.98	3.68	5.85	2.17
40	GIK12392-1	2575	25.17	-16.84	3.54	5.55	2.01
41	KNR166-2 132JPC	0739	24.85	-79.29	1.99	3.45	1.46
42	KNR166-2 127JPC	0631	24.77	-79.27	1.90	3.15	1.25
43	BOFS26/6K	3680	24.45	-19.83	3.12	5.85	2.73
44	KNR166-2 26JPC	0546	24.33	-83.25	1.97	2.85	0.88
45	KNR166-2 29JPC	0648	24.29	-83.27	2.18	3.15	0.97
46	KNR166-2 31JPC	0751	24.22	-83.30	2.38	3.60	1.22
47	GIK12379-3	2136	23.13	-17.74	2.95	5.25	2.30
48	GIK16017-2	0812	21.24	-17.80	2.88	3.75	0.87
49	GIK16030-1	1516	21.23	-18.05	3.08	4.65	1.57
50	GIK12328-5	2778	21.14	-18.57	4.32	5.55	1.23
51	GeoB7920-2	2278	20.75	-18.58	3.06	5.25	2.19
52	BOFS29/1K	4000	20.51	-21.11	3.07	5.85	2.78
53	BOFS30/3K	3580	19.74	-20.72	3.14	5.85	2.71
54	GIK12329-6	3320	19.36	-18.93	2.91	5.55	2.64
55	BOFS31/1K	3300	18.99	-20.16	3.23	5.55	2.32
56	V30-49	3093	18.43	-21.08	3.32	5.55	2.23
57	GIK13289-2	2485	18.07	-18.00	2.95	5.25	2.30
58	108-659	3082	18.07	-21.02	2.83	5.55	2.72
59	GIK12337-5	3082	15.95	-18.13	3.31	5.55	2.24

Table 8 — *Continued*

60	GeoB9508-5	2384	15.49	-17.94	3.36	5.25	1.89
61	GIK16402-1	4203	14.41	-20.56	3.50	5.85	2.35
62	GIK13239-1	3156	13.87	-18.31	3.54	5.55	2.01
63	GeoB9526-5	3223	12.43	-18.05	3.40	5.55	2.15
64	M35003-4	1299	12.09	-61.24	2.01	4.65	2.64
65	V28-122	3623	11.93	-78.68	3.13	5.85	2.72
66	V28-127	3237	11.65	-80.13	3.69	5.55	1.86
67	68-502	3051	11.49	-79.37	2.96	5.55	2.59
68	GIK16415-1	3841	09.56	-19.10	3.29	5.85	2.56
69	GeoB9528-3	3057	09.16	-17.66	3.70	5.55	1.85
70	GIK16408-2	4239	09.01	-21.45	2.85	5.85	3.00
71	GIK16459-1	4835	07.27	-26.18	3.37	5.85	2.48
72	EN066-10PG	3527	06.64	-21.89	2.92	5.85	2.93
73	EW9209-1JPC	4056	05.90	-44.19	3.63	5.85	2.22
74	EW9209-1JPC	4056	05.90	-44.19	3.63	5.85	2.22
75	EN066-16PG	3160	05.45	-21.14	3.09	5.55	2.46
76	GIK16457-1	3291	05.39	-21.72	3.17	5.55	2.38
77	GIK16455-1	4160	05.27	-22.86	3.40	5.85	2.45
78	KNR110-55	4556	04.94	-42.89	3.70	5.85	2.15
79	EN066-38PG	2937	04.91	-20.49	3.17	5.55	2.38
80	KNR110-50	3995	04.86	-43.20	3.41	5.85	2.44
81	GIK16856-2	2861	04.80	03.40	2.41	5.55	3.14
82	KNR110-58	4341	04.79	-43.03	3.32	5.85	2.53
83	KNR110-91	3810	04.76	-43.30	3.81	5.85	2.04
84	GIK16453-2	2675	04.73	-20.94	2.91	5.55	2.64
85	KNR110-66	3547	04.56	-43.38	3.40	5.85	2.45
86	KNR110-71	3164	04.36	-43.69	3.62	5.55	1.93
87	KNR110-82	2816	04.33	-43.48	3.30	5.55	2.25
88	EN066-21PG	3792	04.23	-20.62	3.42	5.85	2.43
89	EN066-26PG	4745	03.08	-20.01	3.28	5.85	2.57
90	GIK13521-1	4504	03.02	-22.03	3.11	5.85	2.74
91	EN066-32PG	4998	02.47	-19.73	3.31	5.85	2.54
92	GeoB1101-5	4588	01.65	-10.98	3.62	5.85	2.23
93	V25-59	3824	01.36	-33.48	3.42	5.85	2.43
94	RC13-110	3231	-00.09	-95.65	4.60	5.55	0.95
95	V19-27	1373	-00.46	-82.07	4.17	4.65	0.48
96	GIK16773-1	4662	-00.97	-09.44	3.30	5.85	2.55
97	GeoB1105-4	3225	-01.66	-12.42	3.86	5.55	1.69
98	GIK16867-2	3891	-02.20	05.10	3.03	5.85	2.82
99	GeoB1041-3	4033	-03.47	-07.60	3.34	5.85	2.51
100	GeoB1115-3	2945	-03.56	-12.56	3.28	5.55	2.27
101	GeoB1118-2	4675	-03.56	-16.43	3.44	5.85	2.41
102	GeoB3104-1	0767	-03.66	-37.71	2.70	4.05	1.35
103	GeoB1117-2	3984	-03.81	-14.89	3.47	5.85	2.38
104	BT4	1000	-04.00	10.00	3.08	4.35	1.27
105	GeoB1113-4	2374	-05.74	-11.03	3.64	5.25	1.61
106	GeoB1112-4	3125	-05.77	-10.75	3.18	5.55	2.37

Table 8 — *Continued*

107	175-1078C	0426	-11.92	13.40	2.75	3.15	0.40
108	INMD-115BX	3427	-17.63	-16.21	2.96	5.85	2.89
109	V29-135	2675	-19.70	08.88	3.32	5.55	2.23
110	GeoB1035-3	4450	-21.60	05.03	3.78	6.15	2.37
111	GeoB3202-1	1090	-21.61	-39.97	3.65	4.65	1.00
112	GeoB1034-3	3772	-21.73	05.42	3.63	5.85	2.22
113	RC13-228	3204	-22.33	11.19	3.84	5.85	2.01
114	GeoB1032-3	2505	-22.91	06.03	3.37	5.55	2.18
115	GeoB1211-1	4089	-24.47	07.53	3.08	5.85	2.77
116	GeoB1214-1	3210	-24.69	07.24	4.02	5.85	1.83
117	RC13-229	4194	-26.00	11.00	3.63	5.85	2.22
118	42JPC2012	2296	-27.76	-46.03	3.33	5.55	2.22
119	GeoB1720-3	2004	-28.98	13.83	2.75	5.25	2.50
120	GeoB1720-2	1997	-28.99	13.83	3.66	5.25	1.59
121	54GGC2012	4003	-29.53	-43.33	3.18	5.85	2.67
122	125GGC2012	3589	-29.53	-45.08	4.18	5.85	1.67
123	CHN115-92PC	3934	-30.83	-38.83	3.37	5.85	2.48
124	AII107-131	2925	-31.00	-38.00	3.06	5.55	2.49
125	175-1087A	1371	-31.46	15.31	3.63	4.65	1.02
126	177-1089	4620	-40.93	09.89	2.81	6.15	3.34
127	RC11-83	4718	-41.60	09.71	3.29	6.15	2.86
128	TN057-6	3751	-42.90	08.90	2.06	5.85	3.79
129	TTN057-6-PC4	3725	-42.91	08.60	3.65	5.85	2.20
130	ODP704A	2532	-46.88	07.41	2.80	5.55	2.75
131	177-1094	2807	-53.18	05.13	3.89	5.85	1.96

6.3 Error of Observation

The use of mass spectrometer for the analysis of isotope data introduces a typical analytical error of ±0.1‰ on the benthic foraminiferal oxygen isotopes. This brings about an uncertainty of ±0.4℃ in the temperature. Also, a ±1‰ uncertainty in temperature leads to a ±0.5‰ error in salinity (Labeyrie et al., 1992). The Shackleton et al. (1974) equation (2-2) used in this study is valid only at low temperatures. An additional ±1℃ error is expected in the water temperature due to the general uncertainties in the changing δ_c and δ_w (Labeyrie et al., 1992). Metabolic effects on the $\delta^{18}O$ fractionation is ±0.2‰ which introduces an error of 1.0 to 1.5℃ in the temperature (Spero and Lea, 1996). Diagenesis brings about additional uncertainties on account of dissolution, secondary calcification and recrystallization. There is a difference in temperature of water

surrounding the initial and final burial places which brings about a difference in the $\delta^{18}O$ composition which may or may not be easily rectifiable.

The purpose of this chapter is to evaluate the distribution of active tracers (temperature and salinity), oxygen isotope ratio in seawater (δ_w), and general circulation patterns simulated by CCSM3 plots for the present day with in situ observation from the water column and sedimentary record. For the Younger Dryas, simulated distribution of (δ_c) with CCSM3 are compared for two scenarios, one with additional freshwater forcing following He (2011) and one without, additional freshwater forcing. These simulations are compared with the sedimentary records from Labeyrie et al., 1992, Sarnthein et al., 1994, and the NCDC (http://www.ncdc.noaa.gov/data-access/paleoclimatology-data) and Pangaea (http://pangaea.de/) online databases for surface (0 to 200 m), intermediate (300 to 2000 m), deep (2000 to 4000 m) and bottom water masses (below 4000 m) (Sverdrup and Armbrust, 2008). In addition, stratification in response to different buoyancy forcings are discussed.

Chapter 7

Results

7.1 Present Day CCSM3 Plots

7.1.1. Temperature (T) and Salinity (S) Distribution

In case of temperature (Figure 7-1), the model successfully reproduces the observed surface and intermediate water masses and shows well-defined stratification with a distinct thermocline in the upper 1000 m which is particular characteristic for the tropical and subtropical Atlantic Ocean. Outflow of high saline Mediterranean Sea Water (average salinity ~38.3‰, Talley et al., 2011, textbook) forms a pronounced inclusion in the CCSM3 salinity plot (Figure 7-2, contour interval = 0.2‰). The convergence zones from 50° to 60° in both the North and South Atlanti c (with T = -1° to 2℃, and S = 34.0‰), where the cold, fresh and dense waters from the Arctic and Antarctic Oceans meet the warm, poleward moving equatorial waters, show reasonable agreement with the WOCE plots (Figure 7-3). Both the temperature and salinity CCSM3 plots accurately represent the salty (~36.4‰), very warm (~24℃) low density surface waters near 30°N trapped by the North Atlantic Gyre. Above the NADW (T=2-4℃; S=34.9‰) is the ~9℃) centered at ~1000m depth penetrates the Antarctic Intermediate Water (T=5℃; S=34.4‰), that originates at the Subantarctic front, poleward to about 30°N. .

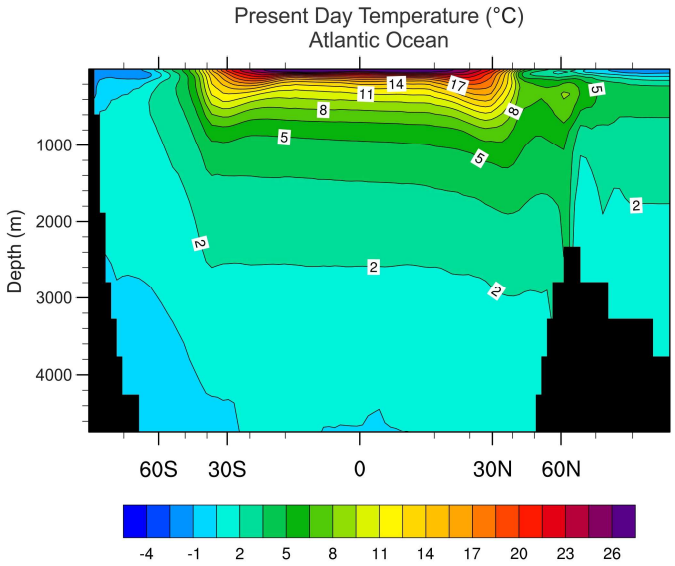

Figure 7-1 Present-day temperature (℃) for the Atl antic Ocean simulated by CCSM3 (contour interval = 1.5℃).

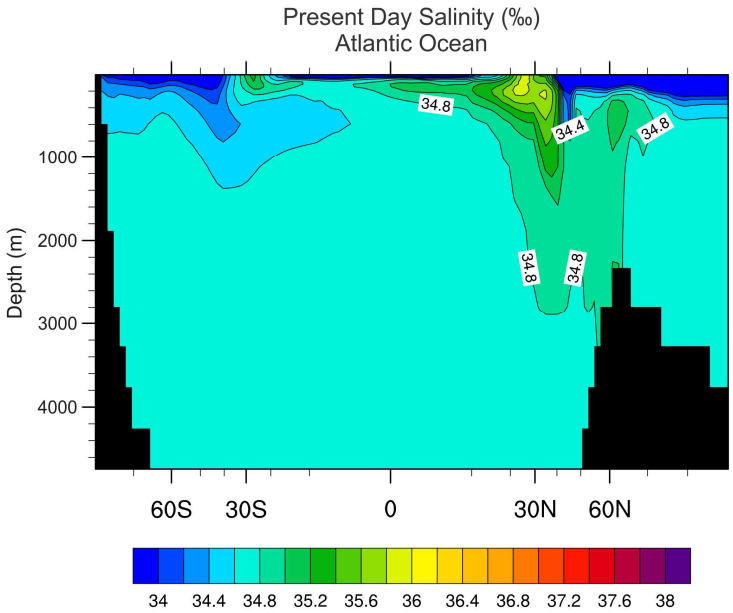

Figure 7-2 Present-day salinity (‰) for Atlantic Ocean simulated by CCSM3 (contour interval = 0.2‰).

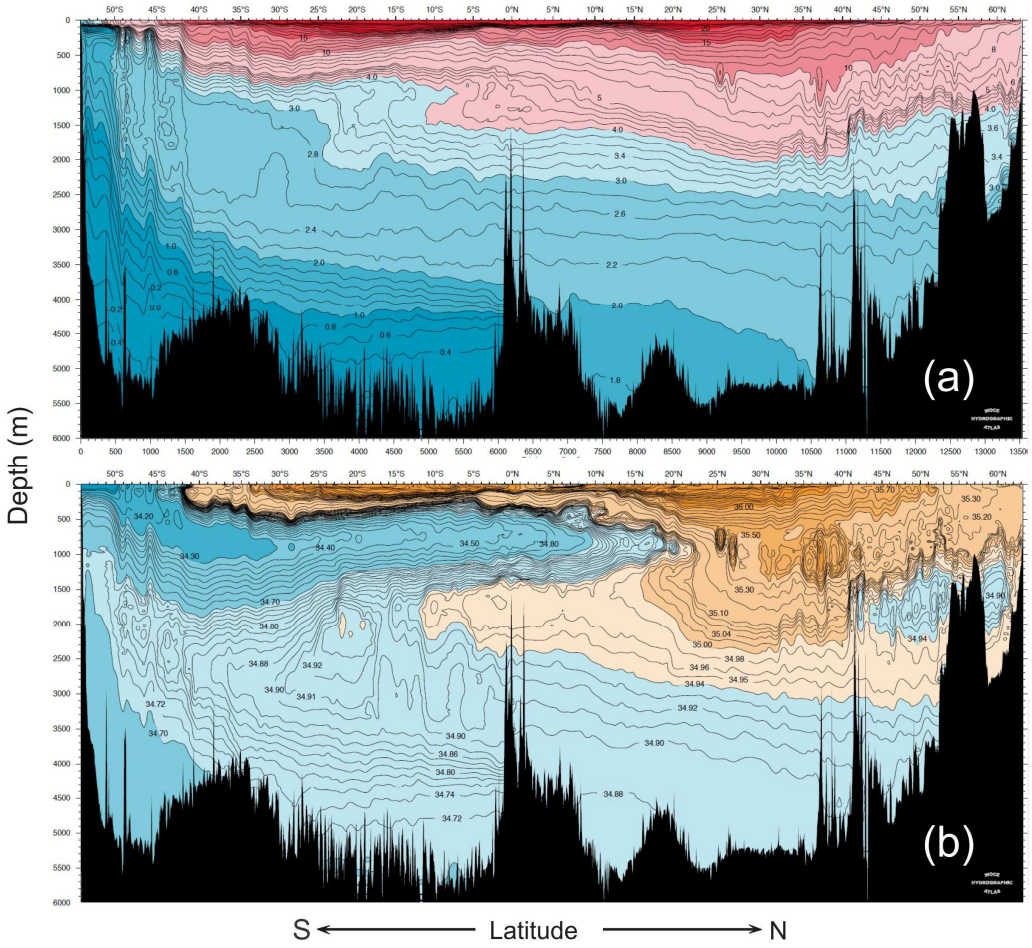

Figure 7-3 Potential temperature (a) and salinity (b) section for the Atlantic Ocean (WOCE Atlas, 2011)

Simulated distribution of salinity in CCSM3 is generally agreeable with WOCE section (consistent salinity values (~34.7‰) below 1500 m and the constant temperature range of 2 to 4℃ that characterize the NADW. The d ensest water in the ocean, Antarctic Bottom Water (AABW) (-0.5℃, 34.8‰), formed near th e edge of Antarctic continent (near 75℃S) seen moving northwards beneath the NADW , is off by around 1‰ in terms of salinity. Overall, the model reproduces the major identifiable patterns of the Atlantic Ocean formed by the temperature and salinity values with an acceptable accuracy.

In comparison to the annual mean surface salinity, World Ocean Atlas (2009) (Figure 7-4), the model is consistent with the polar values (~34.0‰) whereas it tends to be skewed more towards the East American and West African coasts near the equator and tropics compared to the Central Atlantic Ocean.

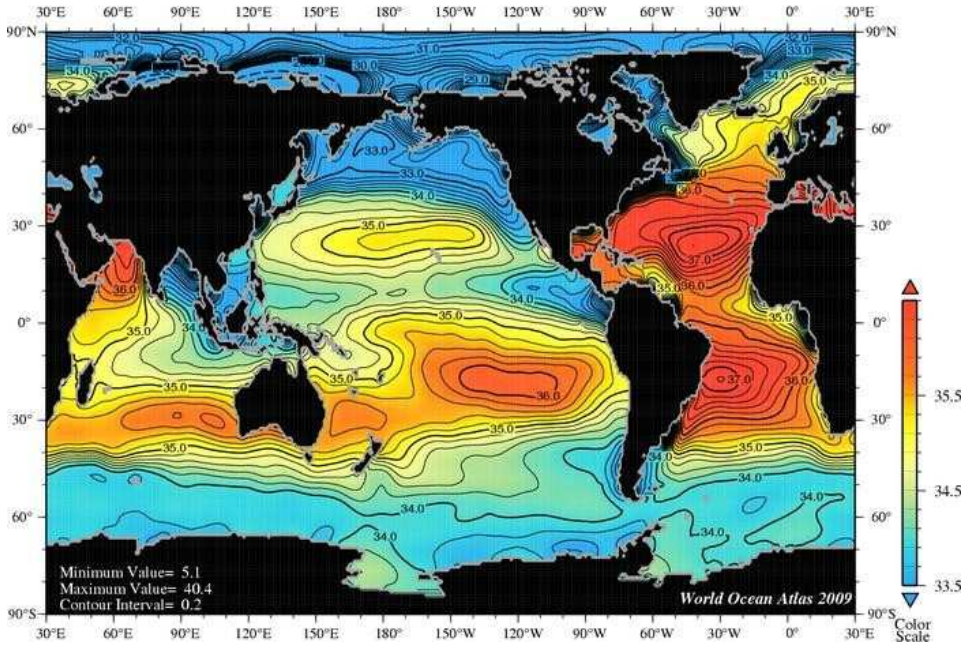

Figure 7-4 Annual mean sea surface salinity (‰) (World Ocean Atlas 2009, Ocean Climate Laboratory) (Contour interval = 0.2‰).

7.1.2. $\delta^{18}O_{SMOW}$ (δ_w) Plot

The gridded dataset $\delta^{18}O_{SMOW}$ (δ_w) (Figure 7-5; LeGrande and Schmidt; 2006), available on the official NASA website (http://data.giss.nasa.gov/o18data/) and the present-day surface δ_w distribution (Figure 7-6) diagnosed from CCSM3 reflects the linear relationship with sea surface salinity $\delta^{18}O$–salinity relationship (Eq. (2-1).

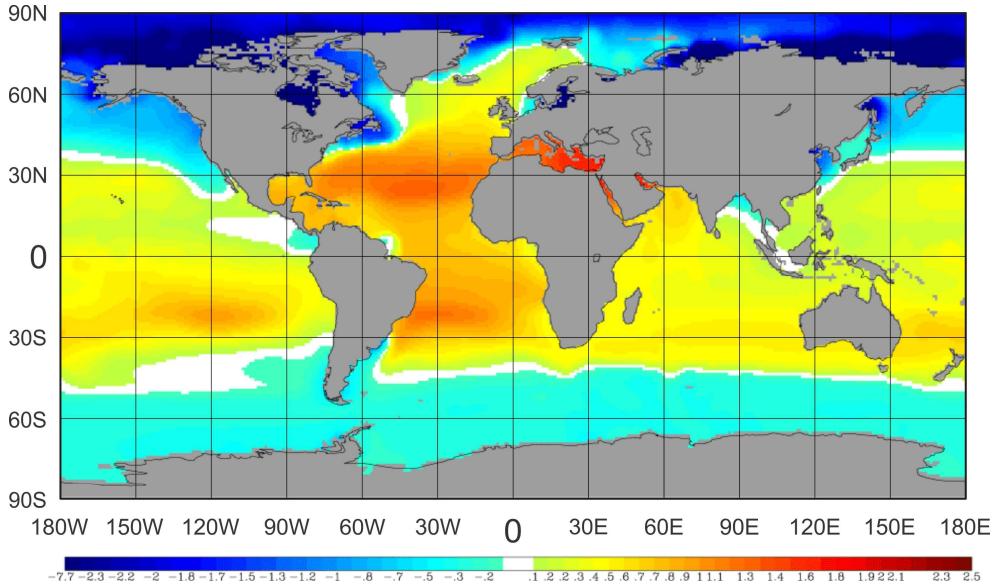

Figure 7-5 Gridded dataset from the values available in the database using regional $\delta^{18}O$ – salinity (‰) relationship (LeGrande and Schmidt; 2006) (Contour interval = 0.1‰)

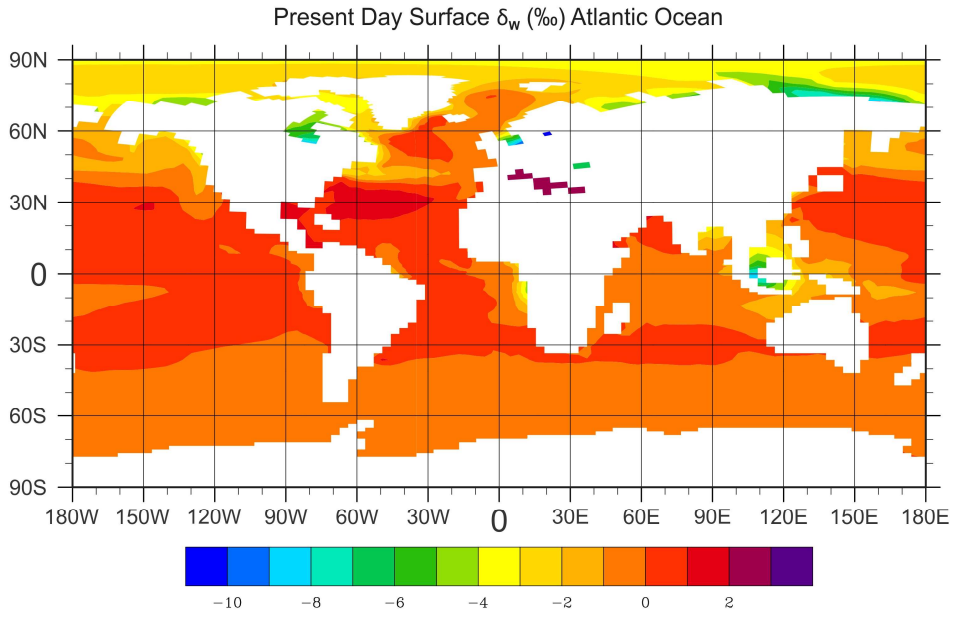

Figure 7-6 Present Day CCSM3 Surface δ_w (contour interval = 1.0‰).

In the following the distribution of δ_w in the Atlantic Ocean surface is discussed keeping in mind the objective of this study. Maximum simulated surface δ_w at 30ºN of

~1.5‰ is overestimated compared to the observed values of 1.35‰. Central Atlantic δ_w values (~1.0‰) are similar to the observed interpolated dataset but waters at the NE tip of the South American coast and the SE coast of African near the equator are considerably lower in the model (-3.5‰ and -4.5‰ in model compared to -0.2‰ and 1.0‰ respectively). Simulated δ_w is -0.5‰ lower at southeastern Greenland compared to the observations. Polar waters are accurately represented in the model with a δ_w of -0.5‰ in the southern ocean and decreasing pole-wards from 0‰ to -3‰ in the northern ocean.

7.1.3. $\delta^{18}O$ Carbonate (δ_c) Plot

For this study the paleotemperature equation ((2-2) given by Shackleton et al. (1974) is inversed to calculate δ_c from temperature, salinity and δ_w. As noted in Yeager et al., 2006 and in 7.1.1. Temperature (T) and Salinity (S) Distribution and 7.1.2. $\delta^{18}O_{SMOW}$ (δ_w) Plot of this chapter, the present day simulated hydrography of the Atlantic Ocean is general agreeable with the observations and thus should also reveal simulated δ_c values (Figure 7-7) close to sedimentary record compiled by Labeyrie et al., 1992 (Table 1) and Sarnthein et al., 1994 (Table 2).

Because of equation (2-2), the diagnosed δ_c correlated highly to the CCSM3 temperature closely in the sea surface and deep sea. Low δ_c values in the North Atlantic around Greenland are representative of NADW origin. There are two dominant intermediate water masses in the Atlantic, namely the Antarctic Intermediate Water (AAIW) and the Mediterranean Intermediate Water (MIW). The AAIW from 0-30°N shows constant δ_c compared to the steep increase in values from 30-50°N (0‰ - 2.8‰). This difference in the gradient can be linked to the MIW. Out of the 20 cores that cover the intermediate water masses, Labeyrie et al., 1992 data shows less error (0.83‰) compared to the Sarnthein et al., 1994 data (1.39‰). The reason for this large error may be a combination of factors such as the CCSM3 coarse resolution model being more

accurate for the surface ocean compared to the intermediate and deep ocean and the difference in analytical techniques used by Labeyrie et al., 1992 and Sarnthein et al., 1994. This error stays constant with depth in case of Labeyrie et al., 1992 and increases with depth for Sarnthein et al., 1994. Three cores from Labeyrie et al., 1992 (V27-60, K11 and V28-38) in the deep North Atlantic waters near 70°N fit well with the δ_c diagnosed from CCSM3 (error 0.08‰, 0.03‰ and 0.07‰ respectively). Highest δ_c values in plot (>4.8‰) are seen in the southern surface waters in the form of a northward protruding AABW. As the Younger Dryas is a Northern Hemisphere climate perturbation, neither of the databases have any cores south of 30°S, making it difficult to confirm the validity of the model in the majority of the Southern Atlantic.

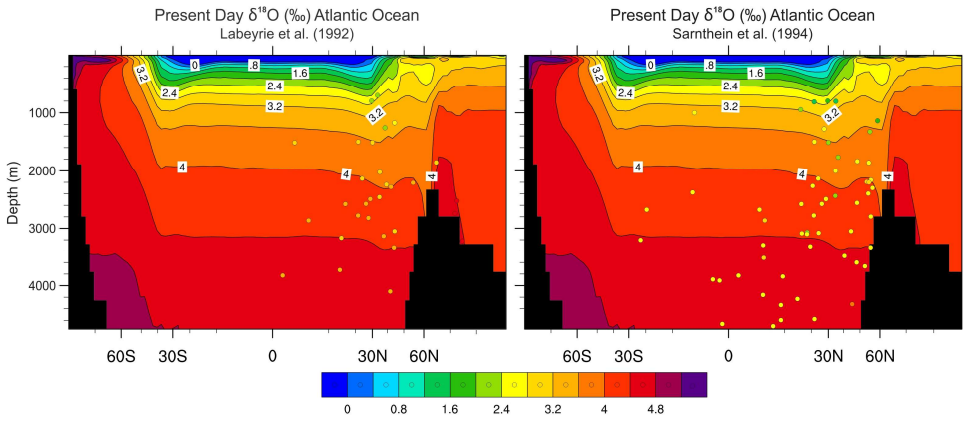

Figure 7-7 Present Day CCSM3 δ_c (‰) plot for the Atlantic Ocean with Labeyrie et al., (1992) (left) and Sarnthein et al., (1994) (right) cores

7.2 Younger Dryas

Two scenarios for the Younger Dryas have been tested, one without freshwater forcing (No FWF) and one with freshwater forcing (FWF) to study the role of freshwater input on the $\delta^{18}O$ distribution at the Younger Dryas. Taylor Hughlett integrated both model runs for approximately 900 years from 13.05 ka (13,050 years before present) to the onset of the Younger Dryas (12.950 ka). For the freshwater forcing simulations,

Bering Strait is kept open and the eastern route via St. Lawrence River is taken as the source of freshwater following He's (2011) PhD. thesis.

7.2.1. Temperature and Salinity Distribution of CCSM3 for the Younger Dryas

Simulated temperature and salinity with and without freshwater forcing for both the Younger Dryas are displayed in Figures 7-8 and 7-9. The most significant changes between these simulations exist north of 40°N. There is an average decrease of ~1.5°C at any given temperature level and an increase of 0.8‰ to 1.0‰ in salinity south of 40°N compared to the present day temperature and salinity plot (Figure 7-1, Figure 7-2) respectively.

For the scenario without the freshwater input surface waters exhibit temperature similar to the one without freshwater throughout the Atlantic. Water masses in the North Atlantic (north of 40°N) are comparatively well vertically ventilated. For the freshwater input scenario, the fresh water input north of 40°N from the St. Lawrence River lead to cold freshwater lens (SST<-1.0°C; SSS <34.0‰) above the denser more saline water masses at intermediate depth. This introduction of freshwater does not seem to significantly alter the subsurface temperature patterns south of 40°N.

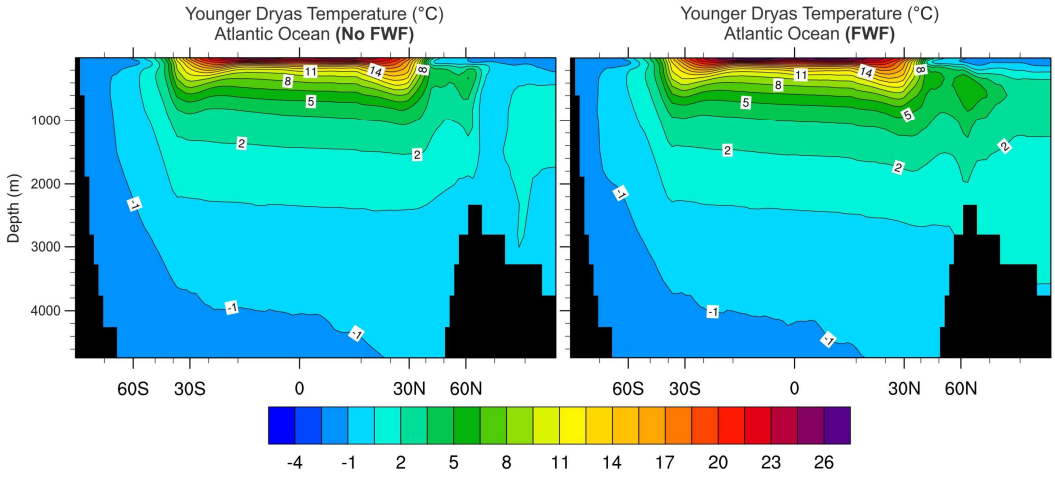

Figure 7-8 Younger Dryas CCSM3 temperature (℃) plo t without (left) and with freshwater forcing (right)

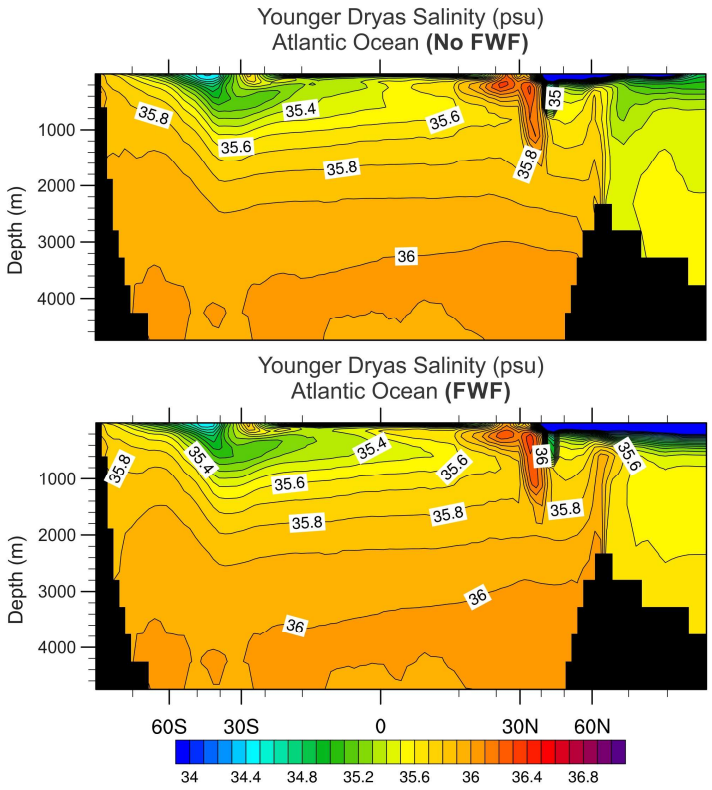

Figure 7-9 Younger Dryas CCSM3 salinity (‰) plot without (top) and with freshwater forcing (bottom)

7.2.1. Diagnosed $\delta^{18}O$ Carbonate (δ_c) Distribution of CCSM3 During the Younger Dryas

The temperature dependency of δ_c is underlined in the structural attributes of the Younger Dryas CCSM3 plots for δ_c as well. South of 50°N, the subsurface configuration is similar in both the scenarios (Figure 7-10 and Figure 7-11) and analogous to the present day (Figure 7-7) configuration when shifted isotopically by approximately +1.0‰. This shift is translated through from the 1.5°C colder intermediate and deep waters (Figure 7-8) compared to present day and is in accordance with the Younger Dryas δ_c values compiled by Labeyrie et al., 1992.

The freshwater pulse form vertically stratified water masses that extend all the way to the Arctic region. This stratification prevents ventilation of deep water below 1200 m, contrary to the scenario without freshwater input. Most of the δ_c data belongs to the North Atlantic to facilitate a reasonable comparison with the freshwater forcing scenario. The lack of data for the surface waters from any of the three databases makes it difficult to validate the model for the upper 300 m of the Atlantic. Overall, the surface and water masses at intermediate depth north of 40°N show lower δ_c values (~4.35‰) in the freshwater input scenario compared to the one without freshwater (~5.25‰) and this is consistent with all the three databases. The CCSM3 plot with freshwater forcing comes closest to Labeyrie et al., 1992 data out of all three, showing least error for both intermediate and deep water masses (0.7‰ and 1.0‰ respectively).

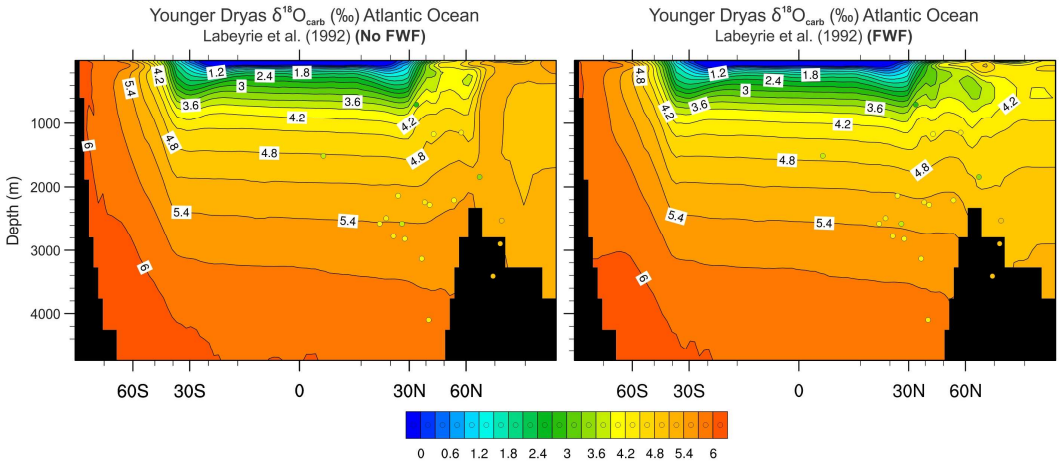

Figure 7-10 Younger Dryas CCSM3 δ_c (‰) plot without (left) and with freshwater forcing (right) with Labeyrie et al., (1992) cores

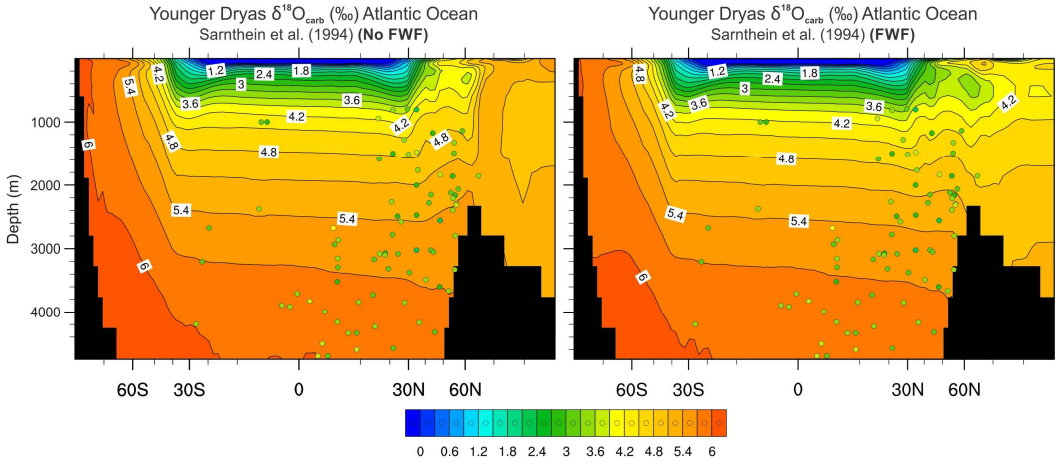

Figure 7-11 Younger Dryas CCSM3 δ_c (‰) plot without (left) and with freshwater forcing (right) with Sarnthein et al., (1994) cores

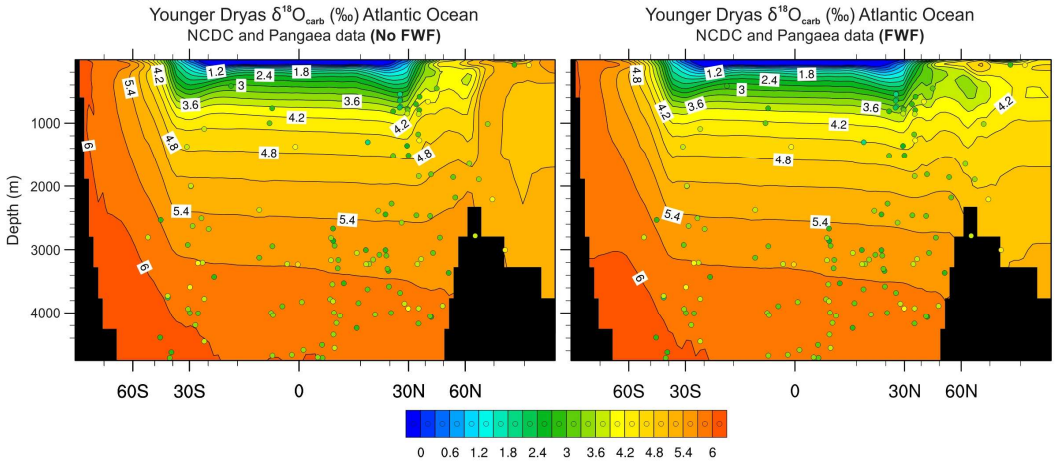

Figure 7-12 Younger Dryas CCSM3 δ_c (‰) plot without (left) and with freshwater forcing (right) with NCDC and Pangaea data

Though the lack of a significant gradient in the Labeyrie et al., 1992 δ_c values below 2100 m is reflected well in the plot, the values themselves are off by ~1.0‰. The significant difference in the model δ_c values and observed δ_c values for deep and bottom waters is related to the δ_w – salinity relationship (2-1) discussed in Chapter 2, 2.5 $\delta^{18}O_{SMOW}$ Inferred from Salinity). The model - data bias increases with depth from the lower NADW to the AABW as also shown in Figure 2-2.

Chapter 8

Discussion

The aim of this chapter is to discuss a few other studies that use similar methodology and involve the use of stable oxygen isotopes from foraminifers to predict paleoclimate conditions. Similar studies applied to different geological times are also discussed.

Mikolajewicz (1996) made use of $\delta^{14}C$ and an idealized $\delta^{18}O$ to facilitate a comparison between the model and sediment core data through sensitivity experiments. Unlike this study, Mikolajewicz used $\delta^{18}O$ as a prognostic tracer. The mean potential temperature and salinity sections produced after achieving a steady state at the end of a 5000 year control run are very similar to the CCSM3 temperature and salinity plots obtained in this study (Figure 7-1 and Figure 7-2). Further, three different freshwater input scenarios with two different sources (Labrador Sea and Mississippi river) for 1500 years each, were employed to check the reproducibility of key climatological events i.e. the collapse of NADW during the Younger Dryas. A total freshwater input equivalent to a global mean sea level rise of 13.4 m was required to cause a rapid termination of the NADW and suppress it for nearly 800 years. It was suggested that the required freshwater input to bring about a collapse was higher than the threshold values.

Similarly, Roche et al. (2003) also employed $\delta^{18}O$ as a passive tracer using a variant of the empirical paleotemperature equation by Shackleton (1974) used in this study. CLIMBER-2, a coarse-resolution, fully coupled, intermediate complexity model is first successfully validated for present day Atlantic, Pacific and Indian Oceans and fluxes from this first experiment are then used to compute the ocean ^{18}O fluxes at the atmosphere-ocean interface during LGM. The $\delta^{18}O_w$ - salinity relationship is more or less

similar for both time periods but LGM is seen to differ in terms of Atlantic deep water $\delta^{18}O_w$ distribution compared to present on account of changes in location of deep water formation.

Xu et al. (2012) used an ocean general circulation model, the Max Planck Institute Ocean Model (MPI-OM), to simulate ^{18}O of seawater and δ_c for the preindustrial and LGM conditions. On comparison they found the ^{18}O preindustrial conditions to be very similar to their simulated LGM conditions except the polar North Atlantic. δ_c for both time periods were found to be in agreement with the observed data. Like Roche et al. (2003), for LGM, ocean-atmosphere boundary was found to be the controlling factor for the oxygen isotopes, whereas the density driven meridional overturning circulation controlled the subsurface features.

Chapter 9

Conclusion

The present-day CCSM3 temperature and salinity plots show a considerably accurate representation of the modern ocean structure. All the major intermediate, deep and bottom water masses are well represented in terms of structure and location. The T31x3 configuration uses pre-industrial initial conditions such as a reduced concentration of well-mixed greenhouse gases as well as a reduced solar constant which represent late Holocene conditions rather than present-day anthropogenic perturbed conditions. This affects the basic physical properties such as temperature and salinity and consequently the model δ_c (Otto-Bliesner et al., 2006). Deep North Atlantic δ_c distribution is generally well reproduced, but significant model data biases exist. Younger Dryas experiments with and without meltwater are structurally differentiated mainly north of 40°N and compared to present day, an overall drop in temperature of ~1.5°C is seen. A corresponding drop of ~+1.0‰ in Younger Dryas δ_c values is seen which is in accordance with findings of Labeyrie et al., 1992. The δ_w – salinity relationship for both present day and Younger Dryas is well maintained. Over all, the simulated Younger Dryas δ_c with freshwater forcing from the St. Lawrence route fits better to the compiled sedimentary record supporting previous studies of Broecker et al. (1985) that a massive meltwater involvement in the North Atlantic at the beginning of the Younger Dryas. It is debatable from the findings that outflow through St. Lawrence is the major route for the fresh water pulse or if meltwater forcing applied is adequate for the onset of such a cold period. Signs of weakening of the AMOC and diminishing of NADW are visible but not definitive.

A similar analysis of an additional proposed eastern route through Mississippi River and the northern Mackenzie River route with a broader and unified database would

be desirable to better understand the onset of Younger Dryas. A longer integration time with multiple freshwater sources and varied forcing scenarios would definitely give an understanding of the North Atlantic circulation during the Younger Dryas.

References

Alley, R.B., 2007, Wally was right: Predictive ability of the North Atlantic “conveyor belt” hypothesis for abrupt climate change: Annu.Rev.Earth Planet.Sci., v. 35, p. 241-272.

Andrews, J.T., and MacLean, B., 2003, Hudson Strait ice streams: a review of stratigraphy, chronology and links with North Atlantic Heinrich events: Boreas, v. 32, p. 4-17.

Atkinson, T., Briffa, K., and Coope, G., 1987, Seasonal temperatures in Britain during the past 22,000 years, reconstructed using beetle remains: Nature, v. 325, p. 587-592.

Bakke, J., Lie, Ø., Heegaard, E., Dokken, T., Haug, G.H., Birks, H.H., Dulski, P., and Nilsen, T., 2009, Rapid oceanic and atmospheric changes during the Younger Dryas cold period: Nature Geoscience, v. 2, p. 202-205.

Belanger, P.E., Curry, W.B., and Matthews, R., 1981, Core-top evaluation of benthic foraminiferal isotopic ratios for paleo-oceanographic interpretations: Palaeogeography, Palaeoclimatology, Palaeoecology, v. 33, p. 205-220.

Berger, W., Killingley, J., Metzler, C., and Vincent, E., 1985, Two-step deglaciation: ^{14}C-Dated high-resolution $\delta^{18}O$ records from the tropical Atlantic Ocean: Quaternary Research, v. 23, p. 258-271.

Bitz, C.M., and Lipscomb, W.H., 1999, An energy-conserving thermodynamic model of sea ice: Journal of Geophysical Research: Oceans (1978–2012), v. 104, p. 15669-15677.

Broecker, W.S., 2006, Was the Younger Dryas triggered by a flood? Science, v. 312, p. 1146-1148.

Broecker, W.S., 1999, What if the conveyor were to shut down? Reflections on a possible outcome of the great global experiment: GSA Today, v. 9, p. 1-7.

Broecker, W.S., Denton, G.H., Edwards, R.L., Cheng, H., Alley, R.B., and Putnam, A.E., 2010, Putting the Younger Dryas cold event into context: Quaternary Science Reviews, v. 29, p. 1078-1081.

Broecker, W.S., Peteet, D.M., and Rind, D., 1985, Does the ocean-atmosphere system have more than one stable mode of operation? Nature, v. 315, p. 21-26.

CCSM3.0 User's Guide. Community Climate System Model National Center for Atmospheric Research, Boulder, CO.

Collins, W.D., Bitz, C.M., Blackmon, M.L., Bonan, G.B., Bretherton, C.S., Carton, J.A., Chang, P., Doney, S.C., Hack, J.J., and Henderson, T.B., 2006, The community climate system model version 3 (CCSM3): Journal of Climate, v. 19, p. 2122-2143.

Coope, G., and Lemdahl, G., 1995, Regional differences in the Late glacial climate of northern Europe based on coleopteran analysis: Journal of Quaternary Science, v. 10, p. 391-395.

Craig, H., 1965, The measurement of oxygen isotope paleotemperatures: Stable Isotopes in Oceanographic Studies and Paleotemperatures, v. 23.

Craig, H., 1961, Standard for reporting concentrations of deuterium and oxygen-18 in natural waters: Science, v. 133, p. 1833-1834.

Dansgaard, W., 1961, The Isotopic Composition of Natural Waters with Special Reference to the Greenland Ice Cap., Meddelelser om Grenland, Bd. 165, Nr. 2.

Dickinson, R.E., Oleson, K.W., Bonan, G., Hoffman, F., Thornton, P., Vertenstein, M., Yang, Z., and Zeng, X., 2006, The Community Land Model and its climate

statistics as a component of the Community Climate System Model: Journal of Climate, v. 19, p. 2302-2324.

Doney, S.C., Lindsay, K., Fung, I., and John, J., 2006, Natural variability in a stable, 1000-yr global coupled climate-carbon cycle simulation: Journal of Climate, v. 19, p. 3033-3054.

Duplessy, J., Labeyrie, L., Juilletleclerc, A., Maitre, F., Duprat, J., and Sarnthein, M., 1991, Surface salinity reconstruction of the North-Atlantic ocean during the last glacial maximum: Oceanologica Acta, v. 14, p. 311-324.

Duplessy, J.C., Lalou, C., and Vinot, A.C., 1970, Differential isotopic fractionation in benthic foraminifera and paleotemperatures reassessed: Science, v. 168, p. 250-251.

Eisenman, I., Bitz, C.M., and Tziperman, E., 2009, Rain driven by receding ice sheets as a cause of past climate change: Paleoceanography, v. 24.

Emiliani, C., 1971, Depth habitats of growth stages of pelagic foraminifera: Science, v. 173, p. 1122-1124.

Epstein, S., and Mayeda, T., 1953, Variation of O18 content of waters from natural sources: Geochimica Et Cosmochimica Acta, v. 4, p. 213-224.

Firestone, R.B., West, A., Kennett, J., Becker, L., Bunch, T., Revay, Z., Schultz, P., Belgya, T., Kennett, D., and Erlandson, J., 2007, Evidence for an extraterrestrial impact 12,900 years ago that contributed to the megafaunal extinctions and the Younger Dryas cooling: Proceedings of the National Academy of Sciences, v. 104, p. 16016-16021.

Hunke, E., and Dukowicz, J., 1997, An elastic-viscous-plastic model for sea ice dynamics: Journal of Physical Oceanography, v. 27, p. 1849-1867.

Joos, F., and Spahni, R., 2008, Rates of change in natural and anthropogenic radiative forcing over the past 20,000 years: Proceedings of the National Academy of Sciences, v. 105, p. 1425-1430.

Kendall, C., and McDonnell, J.J., 1998, Isotope Tracers in Catchment Hydrology: Amsterdam, Elsevier Science B.V., Developments in Water Science, p. 319-346.

Kennett, D.J., Kennett, J.P., West, A., West, G.J., Bunch, T.E., Culleton, B.J., Erlandson, J.M., Hee, S.S.Q., Johnson, J.R., and Mercer, C., 2009, Shock-synthesized hexagonal diamonds in Younger Dryas boundary sediments: Proceedings of the National Academy of Sciences, v. 106, p. 12623-12628.

Kennett, D.J., Kennett, J., West, A., Mercer, C., Hee, S.Q., Bement, L., Bunch, T., Sellers, M., and Wolbach, W., 2009, Nanodiamonds in the Younger Dryas boundary sediment layer: Science, v. 323, p. 94-94.

Labeyrie, L.D., Duplessy, J., Duprat, J., Juillet-Leclerc, A., Moyes, J., Michel, E., Kallel, N., and Shackleton, N.J., 1992, Changes in the vertical structure of the North Atlantic Ocean between glacial and modern times: Quaternary Science Reviews, v. 11, p. 401-413.

LeCompte, M.A., Goodyear, A.C., Demitroff, M.N., Batchelor, D., Vogel, E.K., Mooney, C., Rock, B.N., and Seidel, A.W., 2012, Independent evaluation of conflicting microspherule results from different investigations of the Younger Dryas impact hypothesis: Proceedings of the National Academy of Sciences, v. 109, p. E2960-E2969.

LeGrande, A.N., and Schmidt, G.A., 2006, Global gridded data set of the oxygen isotopic composition in seawater: Geophysical Research Letters, v. 33, p. L12604.

Liu, Z., Otto-Bliesner, B., He, F., Brady, E., Tomas, R., Clark, P., Carlson, A., Lynch-Stieglitz, J., Curry, W., and Brook, E., 2009, Transient simulation of last

deglaciation with a new mechanism for Bølling-Allerød warming: Science, v. 325, p. 310-314.

Mangerud, J., Gulliksen, S., and Larsen, E., 2010, 14C-dated fluctuations of the western flank of the Scandinavian Ice Sheet 45–25 kyr BP compared with Bølling–Younger Dryas fluctuations and Dansgaard–Oeschger events in Greenland: Boreas, v. 39, p. 328-342.

McCorkle, D.C., Emerson, S.R., and Quay, P.D., 1985, Stable carbon isotopes in marine porewaters: Earth and Planetary Science Letters, v. 74, p. 13-26.

Mikolajewicz, U., 1996, A Meltwater Induced Collapse of the "conveyor belt" Thermohaline Circulation and Its Influence on the Distribution of [Delta] 14C and [delta] 18O in the Oceans: Max-Planck-Institut für Meteorologie.

Mix, A., 1987, The oxygen-isotope record of glaciation: The Geology of North America, v. 3, p. 111-135.

Murton, J.B., Bateman, M.D., Dallimore, S.R., Teller, J.T., and Yang, Z., 2010, Identification of Younger Dryas outburst flood path from Lake Agassiz to the Arctic Ocean: Nature, v. 464, p. 740-743.

Najjar, R., and Orr, J., 1999, Biotic-HOWTO: Internal OCMIP Report, LSCE/CEA Saclay, Gifsur-Yvette, France.

Otto-Bliesner, B.L., Tomas, R., Brady, E.C., Ammann, C., Kothavala, Z., and Clauzet, G., 2006, Climate sensitivity of moderate-and low-resolution versions of CCSM3 to preindustrial forcings: Journal of Climate, v. 19, p. 2567-2583.

Östlund H.G., Craig, C., Broecker, W.S., and Spencer, D., 1987, GEOSECS Atlantic, Pacific, Indian Ocean Expeditions. Shorebased Data and Graphics. GEOSECS Atlas Series, Volume 7, 200, U.S. Government Printing Office, Washington D.C.

Peltier, W., 2004, Global glacial isostasy and the surface of the ice-age Earth: The ICE-5G (VM2) model and GRACE: Annu.Rev.Earth Planet.Sci., v. 32, p. 111-149.

Peltier, W., Vettoretti, G., and Stastna, M., 2006, Atlantic meridional overturning and climate response to Arctic Ocean freshening: Geophysical Research Letters, v. 33, p. L06713.

Pinter, N., Scott, A.C., Daulton, T.L., Podoll, A., Koeberl, C., Anderson, R.S., and Ishman, S.E., 2011, The Younger Dryas impact hypothesis: A requiem: Earth-Science Reviews, v. 106, p. 247-264. Redfield, A.C., 1963, The influence of organisms on the composition of sea water: The Sea, p. 26-77.

Robin, G.d.Q., 1977, Ice cores and climatic change: Philosophical Transactions of the Royal Society of London.B, Biological Sciences, v. 280, p. 143-168.

Roche, D., Paillard, D., Ganopolski, A., and Hoffmann, G., 2003, Modelled ^{18}O-salinity relationship for present-day and LGM: Equilibria simulations in a coupled climate model of intermediate complexity, in EGS-AGU-EUG Joint Assembly, abstract no. 5042.

Rooth, C., 1982, Hydrology and ocean circulation: Progress in Oceanography, v. 11, p. 131-149.

Ruddiman, W.F., and McIntyre, A., 1981, The North Atlantic Ocean during the last deglaciation: Palaeogeography, Palaeoclimatology, Palaeoecology, v. 35, p. 145-214.

Ruddiman, W.F., Sancetta, C., McIntyre, A., Manley, G., Dreimanis, A., and Lamb, H., 1977, Glacial/Interglacial Response Rate of Subpolar North Atlantic Waters to Climatic Change: The Record in Oceanic Sediments [and Discussion]: Philosophical Transactions of the Royal Society of London.B, Biological Sciences, v. 280, p. 119-142.

Schrag, D., and DePaolo, D., 1993, Determination of $\delta^{18}O$ of seawater in the deep ocean during the Last Glacial Maximum: Paleoceanography, v. 8, p. 1-6.

Shackleton, N.J., and Opdyke, N.D., 1973, Oxygen isotope and palaeomagnetic stratigraphy of Equatorial Pacific core V28-238: Oxygen isotope temperatures and ice volumes on a 10^5 year and 10^6 year scale: Quaternary Research, v. 3, p. 39-55.

Shackleton, N., Wiseman, J., and Buckley, H., 1973, Non-equilibrium isotopic fractionation between seawater and planktonic foraminiferal tests: Nature (London), v.242, no.5394, p.177-179.

Shackleton, N., 1974, Attainment of isotopic equilibrium between ocean water and the benthonic foraminifera genus *Uvigerina*: Isotopic changes in the ocean during the last glacial: Colloques Internationaux du Centre National du Recherche Scientifique, v. 219, p. 203–210.

Spero, H.J., and Lea, D.W., 1996, Experimental determination of stable isotope variability in *Globigerina bulloides*: implications for paleoceanographic reconstructions: Marine Micropaleontology, v. 28, p. 231-246.

Stuiver, M., and Grootes, P.M., 2000, GISP2 oxygen isotope ratios: Quaternary Research, v. 53, p. 277-284.

Surovell, T.A., Holliday, V.T., Gingerich, J.A., Ketron, C., Haynes, C.V., Hilman, I., Wagner, D.P., Johnson, E., and Claeys, P., 2009, An independent evaluation of the Younger Dryas extraterrestrial impact hypothesis: Proceedings of the National Academy of Sciences, v. 106, p. 18155-18158.

Talley, L.D., Pickard, G.L., Emery, W.J., and Swift, J.H., 2011, Descriptive physical oceanography: an introduction: Access Online via Elsevier.

Tarasov, L., and Peltier, W., 2005, Arctic freshwater forcing of the Younger Dryas cold reversal: Nature, v. 435, p. 662-665.

Tian, H., Schryvers, D., and Claeys, P., 2011, Nanodiamonds do not provide unique evidence for a Younger Dryas impact: Proceedings of the National Academy of Sciences, v. 108, p. 40-44.

Urey, H.C., 1948, Oxygen isotopes in nature and in the laboratory: Science, v. 108, p. 489-496.

Vinot-Bertouille, A., and Duplessy, J., 1973, Individual isotopic fractionation of carbon and oxygen in benthic foraminifera: Earth and Planetary Science Letters, v. 18, p. 247-252.

Wanninkhof, R., 1992, Relationship between wind speed and gas exchange over the ocean: Journal of Geophysical Research: Oceans (1978–2012), v. 97, p. 7373-7382.

Winn, K., Sarnthein, M., and Erlenkeuser, H., 1991, 18O stratigraphy and chronology of Kiel sediment cores from the east Atlantic: Ber.Geol.-Paläontol.Inst.Mus, v. 45, p. 99.

Winguth, A., Shellito, C., Shields, C., and Winguth, C., 2010, climate response at the Paleocene-Eocene thermal maximum to greenhouse gas forcing-a model study with CCSM3: Journal of Climate, v. 23, p. 2562-2584.

Yeager, S.G., Shields, C.A., Large, W.G., and Hack, J.J., 2006, The low-resolution CCSM3: Journal of Climate, v. 19, p. 2545-2566.

Zahn, R. 1986, Coastal upwelling and deep-water circulation in the northeastern Atlantic during the late quaternary. Stable isotopes evidence. PhD Thesis, Kiel University.

Zhang, G.J., and Wang, H., 2006, Toward mitigating the double ITCZ problem in NCAR CCSM3: Geophysical Research Letters, v. 33, p. L06709.

Biographical Information

Anand Soni was born on the 15th of April, 1985 in the city of Vadodara (Gujarat, India) where he spent the entirety of his childhood and adult life before coming to the United States for further studies. He is the second son to Mukesh and Shubhada Soni.

He acquired his bachelor's and master's degree in Geology from the Maharaja Sayajirao University of Vadodara. During his B.S. he had physics and geography as his minors and carried out primary geological and geomorphological mapping in a metamorphic terrain approximately 100 square km in area complete with nomenclature of rock samples, preparation of geological, geomorphological and drainage maps along with manually preparing thin sections.

As a student he always gravitated to the subject of Geology as it engulfs the fundamentals of all sciences and applies them for the understanding of the basic as well as complex earth processes.